Science of the Total Environment 951 (2024) 175536

Contents lists available at ScienceDirect

Science of the Total Environment

journal homepage: www.elsevier.com/locate/scitotenv

Review

# Predictive modeling of atmospheric nuclear fallout microphysics

D.L. McGuffin *, D.D. Lucas, E. Balboni, J.S. Nasstrom, K.A. Lundquist, K.B. Knight

*Lawrence Livermore National Laboratory, Livermore, CA 94550, USA*

## HIGHLIGHTS

- Current post-detonation nuclear fallout models prescribe particle characteristics.
- Fallout microphysics models can predict effects across diverse conditions.
- Recent advancements in cloud and aerosol microphysics models are applicable to fallout modeling.
- Improved thermodynamics and chemistry knowledge is necessary at relevant conditions.
- Coupling fallout and atmospheric models enhances the fidelity of large-scale impact prediction and interpretation.

## GRAPHICAL ABSTRACT

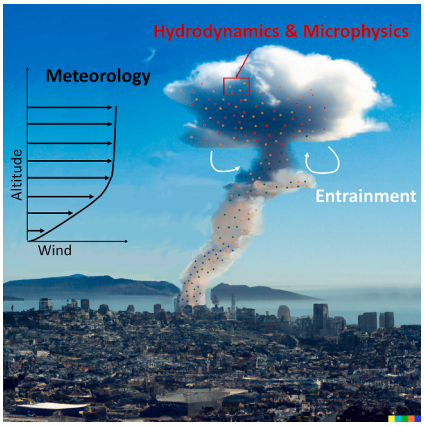


## ARTICLE INFO

Editor: Hai Guo

*Keywords:*
Fallout
Nuclear detonation
Microphysics
Emergency response

## ABSTRACT

The capability to predict size, composition, and transport of nuclear fallout enables public officials to determine immediate and prolonged guidance in the event of a nuclear incident. Predictive computer models of fallout can also provide useful insight for nuclear forensic response when detailed radiochemical processes can be reliably included. Current post-detonation nuclear fallout models prescribe particle size distributions empirically or semi-empirically, based on measurements across limited conditions pertaining to tests conducted primarily in Nevada and the Pacific. These empirical fallout relationships may be subject to large uncertainties in particle size and radionuclide activity distribution if used to extrapolate to other regions with different environmental conditions (e.g., urbanized areas). Replacing empirical relationships with physics-based microphysical process modeling can enable significant advances in the fidelity of predictive models simulating distributions of fallout across diverse environments. Particle *microphysics* describes the formation and evolution of fallout particles, as well as the interaction of radioactive material with entrained particles, which requires accounting for fundamental processes such as nucleation, condensation, and coagulation. The objective of this perspective article is to summarize computational techniques to simulate particle microphysical processes advancing the fidelity of predicting nuclear fallout. We review current empirical models for simulating post-detonation fallout and assess promising research directions moving towards physics-based predictive systems.

* Corresponding author.
*E-mail address:* mcguffin1@llnl.gov (D.L. McGuffin).

https://doi.org/10.1016/j.scitotenv.2024.175536
Received 7 June 2024; Received in revised form 23 July 2024; Accepted 13 August 2024
Available online 21 August 2024

## 1. Introduction: nuclear fallout

In the event of an unexpected nuclear explosion, response may include public health and safety and nuclear forensics. Fallout models support public health and safety by informing assessments of contamination and dose. Nuclear forensics needs may include post-detonation debris for later analysis to inform legal prosecution and other response. Accurate and timely predictions of radionuclide dispersion and distribution are critical to both applications. Model predictions supporting nuclear emergency response include varied outputs such as dose rate, integrated dose, deposited particle size, and fractionation of radionuclides. Current post-detonation nuclear fallout models prescribe fallout size distributions empirically or semi-empirically leading to large uncertainties in model predictions.

Operational fallout models used to make these predictions typically use fast-running source term models that provide a description of the stabilized nuclear cloud, including the distribution of activity among particle sizes and spatially within the initial fallout cloud. Current nuclear detonation source term models use empirical particle size distributions based on observations from low-yield, near-surface tests at the Nevada Nuclear Security Site (NNSS) (Norment, 1979; Harvey and Serduke, 1979), with empirical or simplified physics for determining the cloud geometry, activity-height and activity-size distributions, and other attributes. However, elevated detonations and detonations in different emplacement conditions can produce significantly different dispersion source terms. An example of this is the Grable test, detonated just below the fallout-free height of burst at 160 m above ground. This height of burst resulted in limited entrainment of soil, with a bifurcated cloud, where activity from fission products is concentrated in the cloud cap. As shown in Fig. 1 (reproduced from Lundquist et al. (2023)), the bifurcated nature of the stabilized cloud (1a) is captured when using a cloud rise model solving the governing equations of atmospheric flow (1b). Inclusion of previously neglected physics, including the microphysics of debris formation and its evolution, can lead to improved predictions of dose rate, as shown in Fig. 1c.

Response to a nuclear explosion may also utilize predictions of fallout size and radionuclide ratios, which is the ratio the activity between two deposited radionuclides. This type of prediction can inform public health and safety and help guide sample collection. A widely varying ratio indicates that fractionation occurred in the nuclear explosion and evolving cloud, which results in a difference between the composition of radionuclides produced by the detonation and the composition found in fallout debris. Example products of use when responding to or predicting effects of a nuclear event are shown in Fig. 2 for the Johnnie Boy test detonated at the surface using LODI-DELFIC models described by Lundquist et al. (2023) and briefly introduced in Section 4.2. An understanding of particle size, dispersion, and the radionuclide-based fallout pattern can guide collection strategies. Such predictions currently use simplified fractionation model using empirical particle size distributions, but can be significantly improved by simulating the fallout formation and evolution.

Atmospheric nuclear detonations generate a fireball that quickly cools, rises, and entrains its surroundings (e.g., air, water, soil) to form a mushroom cloud that leaves behind radioactive debris. The effects of a nuclear detonation and the underlying physical phenomena are described by Glasstone and Dolan (1977). Effects include the initial blast and expanding shock wave, thermal radiation emitting light and heat, and nuclear radiation, with explosive energy partitioned among these effects depending on the detonation characteristics (e.g., fissionable material, detonation height and yield) and environment. As the fireball grows, it entrains the surrounding materials (e.g., air, soil, water) and cools, allowing vapors to condense and form radionuclide-laden debris ('fallout'). For near-surface detonations, debris larger than 1 mm, called "ejecta", which contain activation products, quickly fall near ground zero. Later time fallout settles and deposits over timescales ranging from seconds to months depending on the detonation size, detonation height,

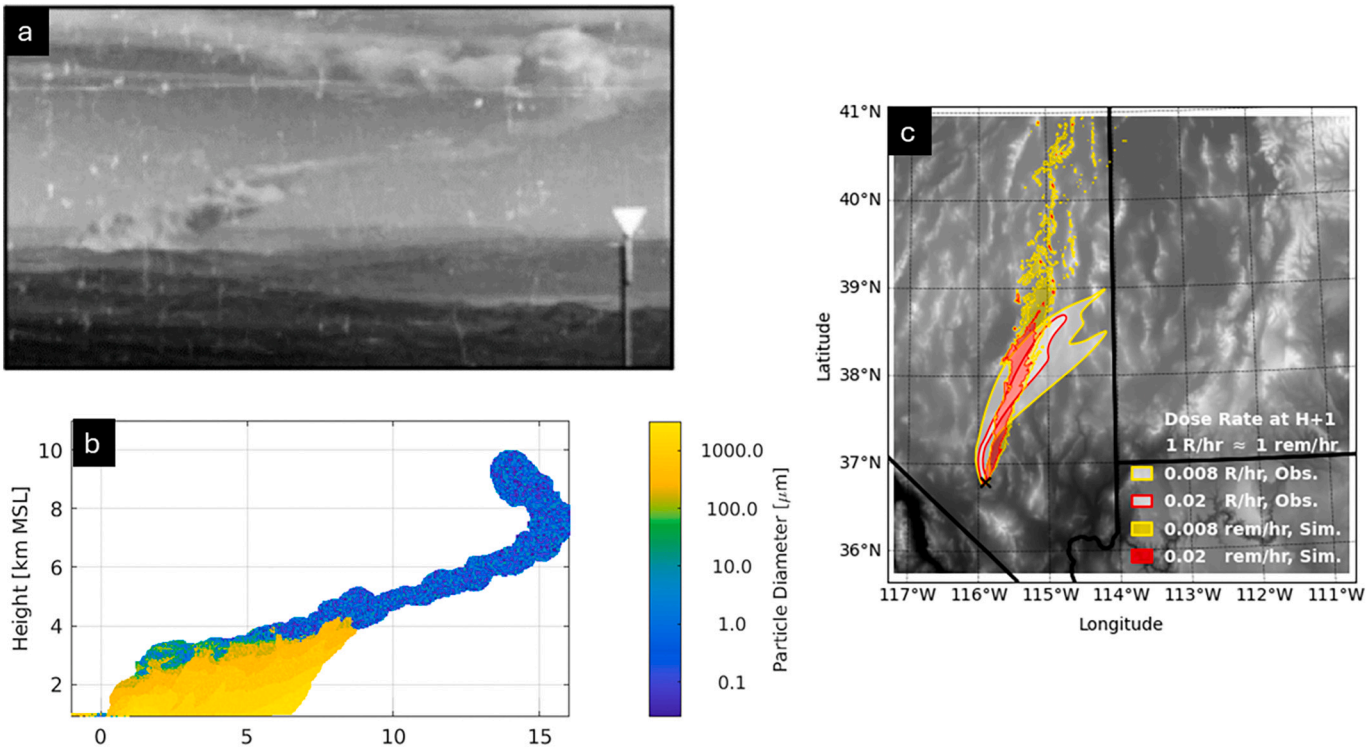


**Fig. 1.** Model predictions of the elevated Grable test are shown compared with observations. A more complex treatment of particle size distribution enables improved correlation between the model and measurements, relative to empirical approaches. Panel a shows the historical image of the bifurcated, stabilized cloud. The fallout model source term for the stabilized cloud is shown (panel b). Observed NNSS offsite exposure rate and model predictions of dose rate contours 1 h post-detonation is shown (panel c). Images shown are reproduced with permission from Lundquist et al. (2023) (see acknowledgments).

and atmospheric processes. Remaining nuclear radiation may be emitted from fallout over an extended period. The immediate and residual hazards associated with fallout formation and dispersion have motivated development of predictive modeling tools to better prepare for and inform planning and response to nuclear emergencies.

Prior work measured fallout of different sizes generated in historic nuclear events and estimated lognormal distributions with geometric mean diameters from 0.065 $\mu$m to 0.21 $\mu$m and mass-weighted median diameters from 4.5 $\mu$m to 302 $\mu$m in samples from high-altitude and near-surface detonations, respectively (Nathans et al., 1970; Heft, 1970). *Early fallout* refers to the large particles with high settling velocities and short airborne lifetimes depositing locally within the first 24 h, in which deposition can extend to a few hundred kilometers downwind depending on the wind speed (Glasstone and Dolan, 1977). *Delayed fallout* refers to the small particles that stay airborne longer than 24 h and are potentially transported for thousands of kilometers before they are scavenged by clouds and precipitation or deposited on the Earth's surface due to gravitational settling and dry deposition. To predict the radioactive contamination from a nuclear detonation, the amount and size of fallout are important characteristics to determine the deposition rates (Machta et al., 1956; Simon et al., 2004). Additionally, the distribution of various radioactive products depends on the particle size through a process known as fractionation, described further below. Accurately modeling the particle size distribution of nuclear fallout to quantify the amount of early and delayed radioactivity deposited is a primary challenge for fallout simulation.

The physical and chemical properties of entrained environmental materials (e.g., minerology, composition, thermodynamic phase, mass, grain size, and density) affect the fallout particle chemistry, size distribution, and the mechanism of explosive energy propagation. Detonations in higher density mediums, i.e., water or soil, partition the fission kinetic energy differently between shock and blast energy and thermal radiation. We follow the convention of distinguishing airbursts from surface bursts where an airburst is detonated high enough above ground so that the fireball at highest radiance does not reach the surface (Glasstone and Dolan, 1977). Fallout from water surface bursts generally produce smaller and lighter particles than land surface bursts since the surroundings mostly consist of water and sea salts. Both water and land surface bursts result in larger fallout sizes than high altitude airbursts that do not vaporize or entrain high density environmental materials. Prior work estimates that land surface bursts result in a larger proportion of early fallout to delayed fallout (roughly 60 % and 40 %, respectively), which is reversed for water surface bursts (30 % and 70 %, respectively) (Ferlic, 1983).

Differences resulting from local environmental factors include examples illustrated in the images shown in Figs. 1a and 2a. These nuclear tests represent the varying types of nuclear event environments. Johnnie Boy was a surface burst and Grable was an airburst with ground-interactions. Fallout clouds from the detonation closer to the surface, i.e., Johnnie Boy, are noted to be darker than airburst clouds (Kuran, 2006; Spriggs et al., 2020), suggesting a difference in cloud composition. Further insights can be gained by considering the scaled height of burst (SHOB, defined by the product of detonation height and yield$^{-1/3}$), which is used to categorize nuclear tests by the level of surface interaction (Spriggs et al., 2020). The scaled heights of burst are roughly $-1$ m kt$^{-1/3}$ and 65 m kt$^{-1/3}$ (meters per kiloton-equivalent of TNT) for Johnnie Boy and Grable, respectively (U.S. Department of Energy, 2015). The increasing scaled height of bursts result in a decreasing mass of soil entrained. Changes in soil entrainment mass and timing can affect overall chemical composition and physical characteristics of fallout and may explain SHOB-correlated observations of cloud appearance.

Particle sizes associated with a nuclear detonation, as with entrainment-driven composition, also vary with the temperature history and timescales of a nuclear detonation. Current fallout codes use empirical particle size distributions to determine the fallout deposition rate (Freiling, 1963). However, microphysical models based on physical principles have been used across several fields, e.g., atmospheric aerosols (Wilson et al., 2001), cloud hydrometeors (Shima et al., 2009), chemical explosions (Sreekanth et al., 2020), and volcanic eruptions (English et al., 2013), to predict particle size distributions. Applying similar microphysics modeling techniques to fallout enables extrapolation to conditions beyond the empirical data. Utilizing a first-principles model of particle microphysics provides predictive fallout size distributions dependent on cloud conditions and the environment. Coupling a model (e.g., hydrocode) with detailed description of the cloud properties including temperature, vapor mass density, and velocity fields to the particle microphysics model can account for complex environments affecting nuclear fallout.

This paper presents approaches to improve predictive fallout microphysics models including chemistry and particle size distribution. We highlight the fundamental microphysical equations governing the formation and evolution of post-detonation fallout in Section 2. In Section 3, we present evidence of microphysical processes from radiochemical debris analyses. Section 4 reviews the current empirical fallout models and discusses alternative numerical methods to capture the evolution of fallout size distributions. Section 5 presents future research

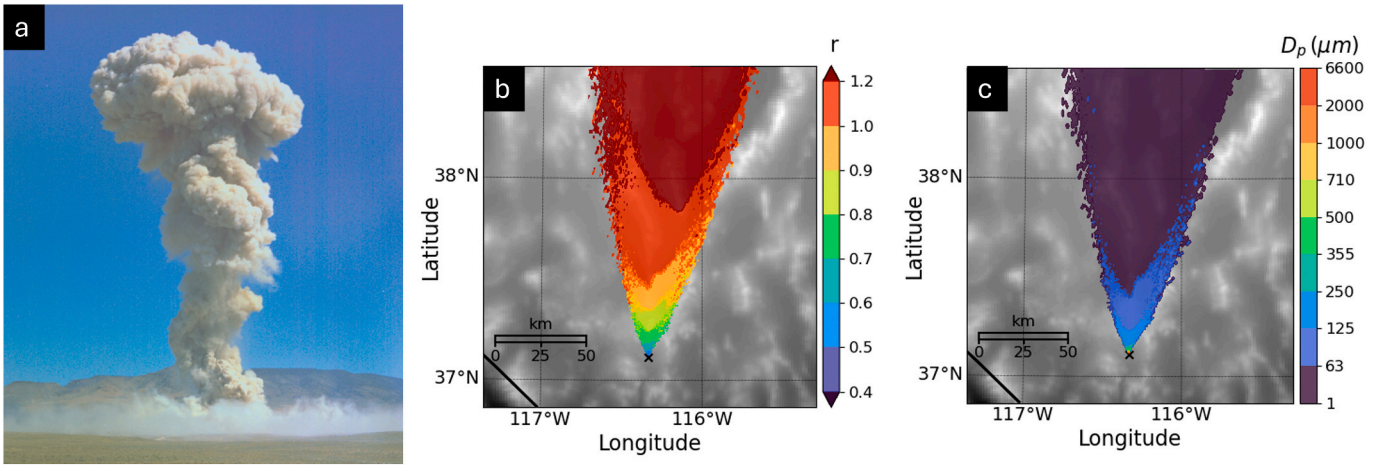


**Fig. 2.** Model predictions of the surface-burst Johnnie Boy event. Historical image of the stabilized cloud is shown in panel a. Fallout model predictions of a ratio of volatile to refractory radionuclides, r, and the mass-weighted mean diameter of deposited particles are shown in panels b and c, respectively. The photograph is reproduced from Spriggs et al. (2020). Model predictions suggest the largest particle sizes are more enriched in refractory radionuclides and show that beyond 50 km, the particles are dominated by small (<63 μm) debris.

applications that can be enabled by coupling fallout microphysics with other systems.

## 2. Fundamental microphysics of fallout evolution

Fallout particles are formed and evolved in fireballs and fallout clouds through the processes of nucleation, condensation, and coagulation. The fireball and mushroom cloud characteristics and dynamics depend on the test magnitude or explosive energy specified by the system yield. As the fireball cools, the vaporized species become supersaturated based on their saturation vapor pressure, nucleating new particles. The nucleated particles grow via condensation of available vapor and coagulation between pre-existing particles. Fallout particles are removed from the atmosphere by wet and dry deposition including precipitation scavenging and gravitational settling. In general, the deposition rate increases as particles grow and gain inertia.

Fallout microphysical processes are modeled with the population balance partial differential equations for the particle size distribution in terms of the population number concentration $n(v,t)$ and each species $i$ mass concentration $m_i(v,t)$ for particle volume $v$ at time $t$ (Seinfeld and Pandis, 2006).

$$\begin{aligned} N(t) &= \int_0^\infty n(v,t)\mathrm{d}v \\ \frac{\partial n(v,t)}{\partial t} &= S_N + J_N + I_N + K_N - R_N \\ A_i(t) &= s_i \int_0^\infty m_i(v,t)\mathrm{d}v \\ \frac{\partial m_i(v,t)}{\partial t} &= S_{M_i} + J_{M_i} + I_{M_i} + K_{M_i} - R_{M_i} \end{aligned} \quad (1)$$

$N$ is the total number concentration of particles, $A_i$ is the total radioactivity of species $i$, and $s_i$ is the intrinsic specific activity of species $i$. Terms in the governing equations represent sources like particle entrainment or radiochemical production $S$, nucleation $J$, vapor condensation to particles $I$, coagulation $K$, and removal due to wet or dry deposition $R$. The subscripts $N$ and $M$ differentiate between the number- and mass-based rates, respectively. These processes are described in the following Sections 2.1 through 2.5.

### 2.1. Mass input

Initially, the energy released by the nuclear detonation vaporizes the device and other materials within the fireball radius. The amount and timing of material entrained is controlled by the detonation height, yield, and surrounding materials. A near-surface burst includes a more complex mixture of materials including soil, water, and air compared to an airburst. Similarly, a larger yield produces a bigger fireball increasing the region of vaporized materials. Both the thermal radiation and shock wave interacting with the surface can facilitate the incorporation of more materials through lofting and sweep-up. The timing of the entrainment of environmental materials is important. Materials introduced later in time, after the vapor has cooled, result in relatively more solids and liquids that act as condensation nuclei instead of a vapor source term. These two options are denoted in the schematic in Fig. 3 with purple dotted arrows. Additional mass input from the ambient environment, like water or oxygen, affect the subsequent microphysical processes. For example, in a marine environment the introduction of water vapor cools the mushroom cloud, which increases the condensation flux as vaporized materials reach their boiling point (Glasstone and Dolan, 1977). The addition of water may also influence the nucleation rate if water vapor stabilizes a critical cluster nuclei. Changes in oxygen availability in above-ground, below-ground, or water environments can also affect the oxidation chemistry and thus the fallout formation and growth rates (Burton et al., 2022; Kwapis et al., 2023). Initial masses as well as the timing and volume of entrained masses all need to be considered when simulating fallout.

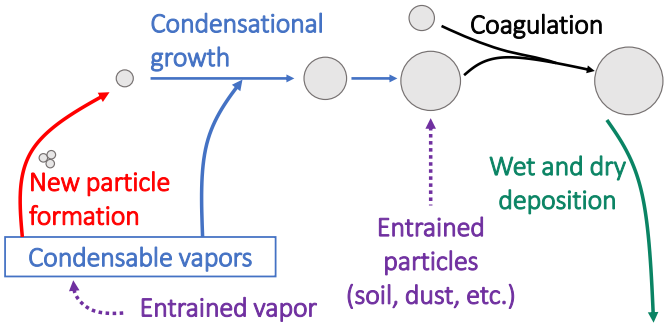


**Fig. 3.** Schematic of fallout microphysics and removal processes contributing to the particle mass and population balances.

### 2.2. Nucleation

As vapor in the hot, fallout cloud becomes supersaturated, liquid or solid particles can nucleate. Classical nucleation theory is often used to estimate the formation rate of new stable clusters from vapor (Farley, 1952). Nucleation rates can be estimated using thermodynamic or kinetic approaches. The thermodynamic approach assumes equilibrium and the capillarity approximation, which approximates the small cluster properties with bulk properties like surface tension $\sigma$ and density $\rho$, to calculate the energy barrier for the formation of a cluster at its critical size ($\Delta G^*$).

$$J = \frac{vN^2}{S}\left(\frac{2\sigma}{\pi m}\right)^{1/2} exp\left(\frac{-\Delta G^*}{k_B T}\right) \quad (2)$$

The thermodynamic model of the nucleation rate $J\,\mathrm{cm}^{-3}\mathrm{s}^{-1}$ is determined from the volume per molecule $v$, concentration of vapor molecules $N$, saturation ratio $S$, mass per molecule $m$, temperature $T$, and Boltzmann constant $k_B$. Alternatively, the kinetic nucleation model explicitly specifies the rate of attachment and detachment of molecules with Arrhenius reaction rates.

If any nuclei seeds are present from the environment or entrained materials, heterogeneous nucleation occurs instead since the additional surface reduces the energy required to form a critical cluster (Liu, 2000). The formation of a nuclei with one species is referred to as homomolecular nucleation while a nuclei with two or more species is heteromolecular nucleation. Heteromolecular nucleation can be more favorable than homomolecular since the combination of different molecular components can reduce the free energy of nucleation. This has been observed in the ambient atmosphere with sulfuric acid and ammonia as well as in stardust with magnesium silicates (Kirkby et al., 2011; Goumans and Bromley, 2012). Heteromolecular and heterogeneous nucleation mechanisms are likely important processes for fallout formation due to particle entrainment and the diversity in radionuclide species.

Available ions, which are produced in abundance in a nuclear fireball, may also enhance nucleation rates by stabilizing the nuclei with electrostatic forces. Two theories describe how ions interact during the nucleation process: ion-mediated and ion-induced nucleation. The classical ion-induced nucleation theory modifies the formation free energy to include electrostatic potential energy while ion-mediated nucleation theory accounts for increased stability and growth of the charged cluster in a kinetic model (Yu et al., 2018). An ion-induced nucleation is likely a significant mechanism of particle formation in a fireball based on work studying thermal plasmas (Girshick, 1994; Vishnyakov et al., 2011). Recent laser ablation experiments are also providing insights into ionization effects in the formation of various oxide species (Taccogna, 2015; Finko et al., 2017; Kautz et al., 2021). Future studies will help elucidate the underlying nucleation mechanisms

for high energy systems like nuclear detonations.

### 2.3. Condensation

Once particles are entrained or nucleated in the fallout cloud, they can act as condensation nuclei for the supersaturated vapor to condense on as the cloud cools. The driving force for condensation depends on the vapor supersaturation $(p_\infty(t)/p_d(t))$ based on the droplet radius $r_d$, available vapor in terms of partial pressure $p_\infty$, and saturation pressure at the droplet surface $p_d$. The saturation pressure $p_d$ depends on the droplet surface tension and accounts for the Kelvin effect barrier to particle growth due to particle curvature.

$$\frac{dM}{dt} = 2\pi r_d \frac{D_v}{R_v T(t)} Nu(r_d)[p_\infty(t) - p_d(t)] \tag{3}$$

The condensation rate $\frac{dM}{dt}$ is based on the vapor diffusion coefficient $D_v$, individual gas constant $R_v$, temperature $T$, and the correction to non-continuum regime with the mass transport Nusselt number $Nu$. Species with differing saturation pressures and diffusivities condense at different times while the cloud cools, which leads to fractionation of debris. The diffusion coefficient utilized is specific to the diffusion of a vapor $v$ through a gaseous medium, like air. Thus, the condensation rate depends on the environment (i.e., underground or underwater) as well as the temperature and pressure conditions. Additionally, the rate of condensation varies throughout the fallout cloud as the vapor pressure and temperature fields are anisotropic.

The volatility of radionuclides produced by the detonation determines whether the radioactivity is surface area- or volume-distributed as radioactive species condense on the surface of solidified particles or evenly distribute throughout a condensate prior to quenching. This can be explained with a time- and volatility-dependent fractionation model, as described in Section 4.1 (Tompkins, 1968). Species are considered volatile when they have a lower boiling point temperature than the solidification temperature of carrier material, and species with higher boiling points are called refractory. The surrounding material entrained in the fallout cloud (e.g., soil, rock, and water) is considered the carrier material for the reference volatility. Fallout composition variability may also result due to continuous condensation within a pre-existing heterogeneous cloud (Lewis et al., 2015).

### 2.4. Coagulation

Coagulation occurs as two particles collide and coalesce forming a new, larger particle. The collision mechanism varies depending on the flow field in addition to particle size, inertia, and settling velocity. As particle size decreases, the particle inertia and settling velocity decrease while their displacement due to diffusion increases so that Brownian motion is the significant cause of coagulation as opposed to particle settling. Additionally, as the flow field transitions from laminar to turbulent, the mechanism transitions from shear flow collisions to accelerative effects of particles deviating from the fluid streamlines (Meyer and Deglon, 2011). Depending on the phase of particles (solid or liquid) at the time of collision, this process may or may not be evident in post-event collected fallout debris. More viscous particles result in agglomeration as an irregular fractal-shaped particle while liquid-phase particles coalescing may result in large spherical particles.

Coagulation is a stochastic process where the probability or rate of collisions is determined by a coagulation kernel, which is a function of the potentially colliding particle sizes (Gillespie, 1975). The coagulation kernel is determined based on the collision mechanism. The general equation for the change in number density of agglomerates $N(r_k)$ based on the coagulation of particles $i$ and $j$ is

$$\frac{dN}{dt}(r_k) = K(r_i, r_j) N(r_i) N(r_j) \tag{4}$$

where $K(r_i, r_j)$ is the coagulation kernel and $N(r_i)$ is the number densities of the colliding particles with radius $r_i$. There are many formulations of the coagulation kernel due to the various collision mechanisms. Any microphysics model attempting to simulate coagulation should include kernels for the significant collision mechanisms including processes such as $K_{dif}$ Brownian diffusion, $K_{sh}$ laminar shear motion, $K_{tur}$ turbulent shear, $K_{set}$ differential settling. Turbulent collision of particles is still an active area of research (Wu et al., 2023), but Eq. (5) provides one example approach as a description for these various collision kernels from Meyer and Deglon (2011).

$$\begin{aligned} K_{dif}(r_i, r_j) &= 4\pi\alpha(r_i, r_j)(D(r_i) + D(r_j))(r_i + r_j)\beta(r_i, r_j) \\ K_{sh}(r_i, r_j) &= \frac{4\Gamma}{3}(r_i + r_j)^3 \\ K_{tur}(r_i, r_j) &= \left(\frac{8\pi\epsilon}{15\nu}\right)^{1/2}(r_i + r_j)^3 \\ K_{set}(r_i, r_j) &= \pi(r_i + r_j)^2 \alpha(r_i, r_j)|V(r_i) - V(r_j)| \end{aligned} \tag{5}$$

Variables used to calculate $K_{dif}$ are the collision efficiency $\alpha$, diffusion coefficient $D(r_i)$, and the Fuchs noncontinuum correction factor $\beta(r_i, r_j)$. Additional variables necessary for other kernels include the velocity gradient $\Gamma$, fluid kinematic viscosity $\nu$, dissipation rate of turbulent kinetic energy per mass $\varepsilon$, and the settling velocity $V(r_i)$. The coagulation kernel may depend on the temperature $T(t)$, mean-free path $\lambda$, the Fuchs non-continuum correction factor, and the turbulent shear rate (Fuchs, 1964). Other potential driving forces of collisions, such as electrostatic forces, may also be a consideration.

### 2.5. Wet and dry deposition

Fallout particles are removed from the atmosphere when they deposit on the surface through wet and dry deposition (with and without precipitation, respectively). The dry deposition velocity for a specific particle size and flow field includes several components, including gravitational settling, inertial impaction, turbulent diffusion, molecular diffusion due to Brownian motion, and phoretic forces, e.g., Emerson et al. (2020). Large particles (e.g., sizes larger than 10 μm) are more quickly deposited due to their fast gravitational settling and large inertia as their trajectories are less influenced by the flow field and fall faster to the surface. As the inertia and particle size (e.g., $< 1$ $\mu$m size) decreases, the deposition velocity decreases, particles follow the flow more closely, and particles stay suspended longer. At sizes less than about 0.1 $\mu$m, however, particles are more affected by Brownian motion and have deposition velocities that increase with decreasing size.

Precipitation (e.g., raindrops, snowflakes) falling through the air can scavenge fallout particles. This “washout” process is more effective for large and heavy particles than small and light particles because the latter can avoid raindrops by following the flow streamlines around the drop. Particles can also serve as cloud condensation nuclei for the formation of cloud and rain droplets. This “rainout” process can be effective for both small and large fallout particles, e.g., Jacobson (2003). Clouds and precipitation form due to rising and cooling air that leads to water vapor condensation. This occurs naturally in the atmosphere but can also occur with the rising fallout cloud itself, particularly in humid environments, in a process known as self-induced rainout (Molenkamp, 1979). The presence of water in the local environment is a necessary consideration for understanding resultant fallout deposition.

A particle's size strongly affects its deposition velocity, such that uncertainties in fallout size distributions can lead to significant differences in the predicted deposition pattern and its correlated chemical (i.e., fractionation) properties. Additionally, smaller particles that stay aloft longer and travel farther become dilute within the atmosphere (and less of a hazard). Predicted exposure rate and location of fallout

properties, e.g., fractionation ratio and particle size, of utility to public health and safety as well as forensic response are strongly affected by the particle deposition velocity and thus the size distribution.

## 3. Fallout debris observations

The fundamental particle microphysical processes governing the formation and evolution of fallout are difficult to directly observe given the extreme temperature and turbulence during a nuclear detonation and immediately following. We can find indirect evidence of these processes, however, by studying samples of historic fallout. Microscopic structures can provide insight to early stages of nucleation and condensation while fallout size and shape can show evidence of growth via condensation and coagulation. Additionally, the debris radioactivity and composition provides insight on the pathway of fallout formation, e.g. vapor condensed on entrained soil or molten debris. Debris samples with irregular shapes composed of agglomerated particles illustrate the coagulation process while tiny spheroidal features illustrate particle nucleation.

Samples of fallout debris have been collected and analyzed to elucidate the underlying microphysical processes that formed the particles prior to depositing. Measurements of the particle composition or radioactivity distribution can provide information about the particle phase when radioactivity was incorporated. Fig. 4 shows three different nuclear debris types from Nevada tests with ground interaction. Samples shown in Fig. 4(a–e) are millimeter-scale local fallout collected on the ground near the detonation location (Weisz et al., 2017; Genda et al., 2021) while Fig. 4(f) debris is micrometer-scale sampled directly from the cloud (Balboni et al., 2022). The debris samples shown were imaged with optical, scanning electron microscope backscatter electron (SEM-BSE), autoradiography, and nanoscale secondary ion mass spectrometry (NanoSIMS). Such methods can provide information on the debris external and internal structure, shape, texture, and chemical composition.

The spherical, aerodynamic fallout sample is shown in Fig. 4(a) and (d) with optical and autoradiography images, respectively. The distribution of radioactivity in the particle is homogeneous, indicating the condensation process played a major role in forming volume-distributed radioactivity prior to solidifying.

The glassy, elongated, aerodynamic sample shown in Fig. 4(b) from a near-surface nuclear test has several smaller aggregated spherical particles fused on the debris surface. The spheroids with an approximate diameter of 185 $\mu$m coagulated with the large, mm-scale, debris. The interface between the host material and an agglomerated spheroid is shown with NanoSIMS measurement in Fig. 4(e). The NanoSIMS image shows the isotope ratio for iron is elevated at the interface. Both U-235 and calcium are elevated relative to silicon in a similar pattern (not shown here), which suggests that vaporized soil or anthropogenic components mixed with device fuel and condensed together (Weisz et al., 2017). Such observations support a continuous condensation-diffusion process with surface-area distributed radioactivity rather than a two-step process with fractionated volatile and refractory species (Weisz et al., 2017) and the subsequent coagulation of small and large particles.

Fig. 4(c) shows the SEM-BSE image from a cross-section of debris formed during a test detonation interacting with an iron tower. The bright pixels show iron-rich regions, which highlight complex textures and morphologies in the rim and interior with an ex-situ amoeboid with core-shell morphology (Genda et al., 2021). These complex internal features demonstrate small-scale microphysical processes such as condensation and potentially nucleation.

Fig. 4(f) represents microscale debris collected by airborne sampling of a fallout cloud from a ground interacting nuclear test. The sample contains a 10 $\mu$m host particle enriched in silicon that likely coagulated with various tiny particles smaller than 2.5 $\mu$m enriched in iron and plutonium, indicating that they may originate from the vapor phase (Balboni et al., 2022).

Historic debris analyses highlight the complexities of nuclear fallout as observed in individual samples. The uniformly distributed radioactivity in Fig. 4(d) suggests well-mixed radionuclides condensing at an earlier time and thus composed of more refractory radionuclides. The surface-distributed radioactivity in Fig. 4(e) may indicate volatile radionuclides condensing on a refractory core. It is hypothesized that early condensates coagulate with molten silicate while radioactive iron vapor condenses (Genda et al., 2021). Under this theory, we see evidence of nucleation and condensation in the nucleated amoeboid with a core-shell geometry seen within the iron-rich rim of Fig. 4(c). Evidence of coagulation is shown by the agglomerate depicted in Fig. 4(b) and (f).

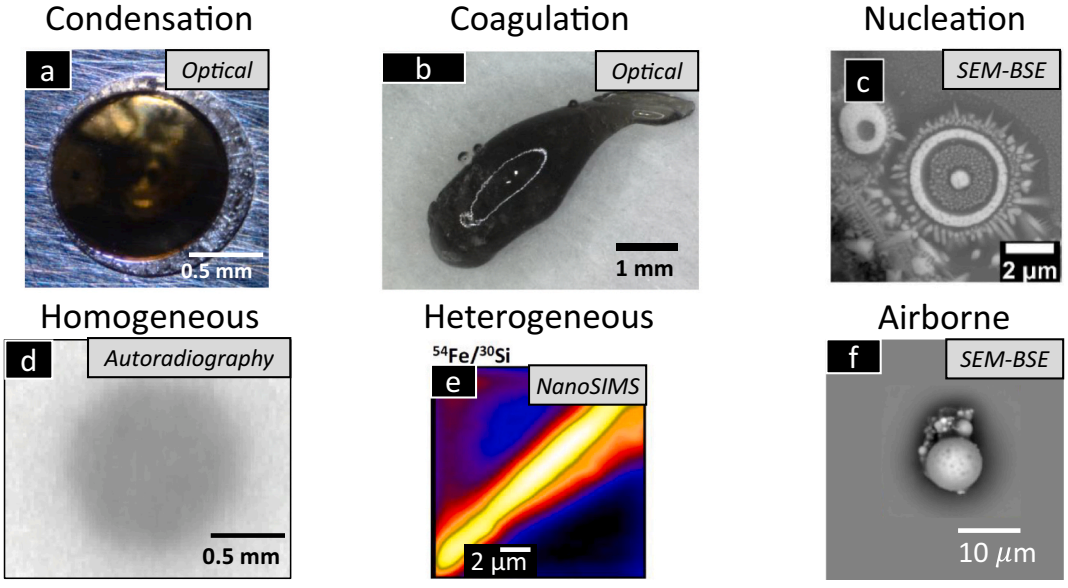


**Fig. 4.** Historic fallout examples illustrating the effects of a) condensation, b) coagulation, and c) nucleation imaged by a variety of methods (see italic text on each image). The bottom row shows examples of debris with d) homogeneous and e) heterogeneous composition as well as f) airborne debris. All debris examples originate from ground-interacting nuclear tests. This selection of observations highlights the complexity of fallout in terms of geometry, composition, and structure. Images shown are reproduced with permission from several publications (see acknowledgments) (Weisz et al., 2017; Genda et al., 2021; Balboni et al., 2022).

While illustrating diversity in fallout, the study of individual samples does not capture the time- and size-dependence of the microphysical processes. A predictive fallout microphysics model would provide more detailed information on the evolution and size distribution of fallout.

## 4. Fallout modeling techniques

Modeling fallout radioactive dose rates and spatial patterns has historically been done with simplified empirical or semi-empirical models that prescribe fallout size distributions in a cloud based on Nevada measurements, without modeling the details of particle microphysical processes. Section 4.1 describes a fractionation model that simplifies the complex behavior of fallout evolution. Section 4.2 describes the current empirically-based, fast-running fallout models. Future modeling techniques for predicting fallout under diverse environments must utilize numerical methods to resolve the microphysical processes and enable extrapolation beyond Nevada measurements. The next Section 4.3 describes the different approaches to capture the fallout formation and evolution in order of increasing complexity.

### 4.1. Empirical fractionation model

Capturing the complex condensation behavior of fallout has historically been approached with simplified models of fractionation based on bulk isotope analysis of fallout debris (Freiling, 1961). Fractionation produces differences between the radionuclide composition in debris samples and the initial radionuclide composition from the detonation. Pathways to fractionation include the various microphysical processes described in Section 2. Prior work predicting fractionation modeling only considers chemical fractionation due to variations in volatility of various radionuclide species. Less volatile radionuclide species condense faster than the carrier material (e.g., soil and rock) resulting in more uniformly-distributed condensates, while more volatile radionuclide species condense later onto the surface of solidified debris entrained later in the cooling history (Miller, 1960). Fractionation is affected by the thermodynamic properties of carrier material entrained or vaporized, as described in Section 2.1. Additionally, the environment affects fractionation chemically since the condensation time and vapor-to-particle flux determines how radionuclides are distributed in fallout as described in Section 2.3. Compounds significant to fallout have diverse volatilities (Hicks, 1982). For example, the boiling point of Molybdenum and Barium is 2619°C and 729°C, respectively, which leads to significant fractionation. Prior work investigated modeling the distribution of radioactivity across particle size with thermodynamic data including the fission product vapor pressures and Henry's law diffusion coefficients (Miller, 1960; Korts and Norman, 1967; Martin, 1983).

The Freiling model (Freiling, 1963) is a widely applied semi-empirical model for fallout particle formation and is useful to predict the activity size distribution and fractionation without explicitly modeling the microphysical processes described in Section 2. This model uses the Freiling Ratio $F_R$ defined as the fraction of the atoms in a fission-product mass chain (which can contain different parent and daughter radionuclides with the same atomic mass number) that are considered refractory relative to the total atoms. Radionuclide species are considered refractory when their boiling point temperature is above a reference boiling point temperature (in the Freiling model the carrier material is considered as the reference), affecting their condensation rates. Based on empirical data, the Freiling model assumes the specific activity (equivalent fissions for a given mass chain per unit mass) within fallout debris is proportional to $D_p^{\sqrt{F_R}-1}$, where $D_p$ is particle diameter (Freiling, 1961). Therefore, for completely refractory mass chains ($F_R$=1), specific activity is constant and the activity-size distribution is volume distributed (or mass distributed for constant particle density). For a wholly volatile mass chain ($F_R$=0) specific activity is proportional to $D_p^{-1}$, which means the activity-size distribution is proportional to $D_p^2$, since specific activity is defined as proportional to $D_p^2/D_p^3 = D_p^{-1}$ (Norment, 1979).

Tompkins (1968) amended the Freiling method so the activity-size distribution for particle diameters larger than a cut-off size of 100 $\mu$m follows a volume-size distribution, independent of the mass chains' volatility, based on fallout observations of specific activity. See Appendix A for a more detailed description of the Freiling-Tompkins semi-theoretical model of fractionation. Predictions using the Freiling-Tompkins model are shown in Figs. 1 and 2 with overall exposure rate from the Grable test and predicted fractionation ratio from the Johnnie Boy test, respectively. Explicitly modeling fallout microphysics can better predict fallout fractionation. While accounting for fractionation can capture significant differences in local fallout chemistry, the total exposure rate (of key importance to public health and safety) may remain unchanged.

### 4.2. Empirical fallout models prescribing size distributions

Fast-running fallout models cannot explicitly include microphysical processes affecting particles due to computational expense, but the models do include processes for particle settling and deposition on the ground. Such models either prescribe empirical particle size distributions for fallout or apply a semi-empirical fractionation model, like Freiling-Tompkins, to determine the fallout size distribution. Typically, fallout sizes are defined by a lognormal distribution across particle diameter with a mean ($\mu$) and standard deviation ($\sigma$). The fallout size distribution can include several modes to represent different types of particles, i.e. a narrow, small size mode for nucleated particles and a wide, large size mode for entrained soil. The number size distribution for particle diameter $D_p$ with $M$ modes and $N_i$ number of particles in the $i^{th}$ mode is described by the equation below.

$$\frac{dN}{dD_p} = \sum_{i=1}^{M} \frac{N_i}{\sqrt{2\pi} D_p \ln\sigma_i} exp\left\{ -\frac{1}{2}\left(\frac{\ln D_p - \ln\mu_i}{\ln\sigma_i}\right)^2 \right\} \quad (6)$$

Some of the empirical fallout models have been assessed and compared (Auxier et al., 2017). The DEfense Land Fallout Interpretive Code (DELFIC) developed at the U.S. Defense Nuclear Agency allows flexibility in specifying the fallout number size distribution. The user can input either tabulated data for a custom size distribution or parameters describing a lognormal or power law representation of the particle number size distribution. The default is a lognormal size distribution based on measurements from the Nevada tests (Norment, 1979).

The Hazard Prediction and Assessment Capability (HPAC) software developed by the Defense Threat Reduction Agency (DTRA) allows the user to choose between applying the size distribution used in DELFIC for surface bursts or the Heft subsurface size distribution, which is composed of three modes for local, glass, and crystalline particles (Skaar, 2005; Heft, 1970). The U.S. Air Force Institute of Technology developed a Fallout Deposition Code (FDC) utilizing Baker's bimodal lognormal size distribution based on measurements from surface bursts, tower-bursts, and airbursts at Nevada (O'Day, 2009; Baker, 1987).

The DELFIC, HPAC, and FDC models require inputs of the fallout *number* size distribution (NSD), but prediction and analysis of fallout is often in terms of the radioactive dose based on the particle *activity* size distribution (ASD). To accomplish this, these models must assume a distribution of radioactivity among particle sizes. DELFIC utilizes the Freiling-Tompkins fractionation model described in Section 4.1, which associates the ASD with the $\left(\sqrt{F_R}+2\right)^{th}$-moment of the NSD for particle diameters below 100 $\mu$m and depends on the radionuclide species post-detonation (Tompkins, 1968). HPAC utilizes the same online calculation of ASD as DELFIC, while the default assumption in FDC is the radioactivity is volume-distributed.

Another fallout modeling approach is to prescribe the fallout ASD. The Department of Defense's Weapons Systems Evaluation Group

(WSEG) developed an analytical "smearing" model WSEG-10 updated in 1982 to include an ASD based on DELFIC that is 68 % volume-distributed and the remaining radioactivity surface-distributed (Bridgman and Bigelow, 1982). The Department of Energy's National Atmospheric Release Advisory Center (NARAC) developed LODIFOC to predict fallout dispersion and deposition using empirical ASD from Nevada measurements (Harvey and Serduke, 1979; Auxier et al., 2017). LODIFOC utilizes the Lagrangian Operational Dispersion Integrator (LODI) code for atmospheric transport and deposition along with stabilized activity-height and activity-size distributions based on empirical parameterizations (Ermak and Nasstrom, 2000; Larson and Nasstrom, 2002; Nasstrom et al., 2007; Sugiyama et al., 2012). The Norwegian Radiation Protection Authority developed the Severe Nuclear Accident Program (SNAP) model, which utilizes a discretized version of the ASD in WSEG-10 (Bartnicki and Saltbones, 2008).

Representing higher heights of bursts requires additional modifications. Existing fallout models represent near-surface bursts (or subsurface bursts for the Heft size distribution) well because most of the data utilized corresponds to near-surface tests. To model higher altitude detonations, DELFIC uses two adjustments: (1) an airburst-specific global-fallout NSD, instead of an near-surface burst NSD, is used when the scaled height of burst, SHOB, is equal to or above a threshold (SHOB $\geq$ 180 ft. kt$^{-1/3.4}$), and (2) a scaling factor that depends on SHOB and reduces the amount of radioactivity on fallout particles for any above-ground burst to account for reduced local fallout for higher heights of burst. LODIFOC, however, retains the total amount of radioactivity on fallout particles, and assumes a larger fraction of the radioactivity is on smaller (delayed fallout) particles for larger scaled heights of burst.

Models make different assumptions about different sources of radioactivity (i.e., neutron activation or fission decay). Ejecta are not typically included in the fallout NSD and ASD, but do contribute to residual radiation. A "ground zero circle" routine in LODIFOC includes ejecta and ground activation products as a source of radioactivity, in addition to fallout. Model assumptions of radioactive sources will translate to radionuclide distribution (e.g., fractionation) and dose pattern uncertainty when used in semi-empirical models.

Fig. 5 shows the cumulative NSD and ASD in the top and bottom panels, respectively, for the fallout models described above. The NSD is not shown for the models that specify the ASD (LODIFOC and SNAP). DELFIC NSD is lognormal with $\mu = 0.407$ $\mu$m and $\sigma = 4$ for near-surface bursts and $\mu = 0.15$ $\mu$m and $\sigma = 2$ for pure airbursts. The DELFIC ASD varies as it is determined by online Freiling-Tompkins fractionation based on the radionuclide composition, soil composition, and detonation characteristics like yield. One example of the DELFIC ASD for a near-surface burst is shown in the bottom panel of Fig. 5 in which the ASD corresponds to 68 % and 32 % volume- and surface-distributed fallout, respectively. HPAC applies an online fractionation calculation to determine the ASD from the Heft NSD, so the Heft ASD shown here assumes 68 % volume-distributed radioactivity from the WSEG-10 fit to DELFIC. SNAP implements 10 tabulated size sections with equal radioactivity based on the DELFIC ASD. The FDC NSD shown is 70 % local fallout based on Baker's NSD, which is assumed to be volume-distributed to determine the ASD. WSEG-10 ASD is not shown since it is equivalent to DELFIC ASD. The median particle diameter among these different fallout codes varies by a about an order of magnitude for the ASD and NSD, as shown by the diameter corresponding to 50 % of the total radioactivity or number concentration. Similar NSD can result in ASD with dramatic differences which, in turn, translates to distinctive estimation of transport and ground deposition including dose rate on the ground.

Variability in how ASD and NSD are represented among the different models is a primary uncertainty in fallout deposition distribution predictions. This uncertainty may be reduced by moving to models that predict fallout microphysics. An advantage of fallout models utilizing empirically-based size distributions is that their predictions match historic fallout deposition patterns at Nevada reasonably well. Prior work

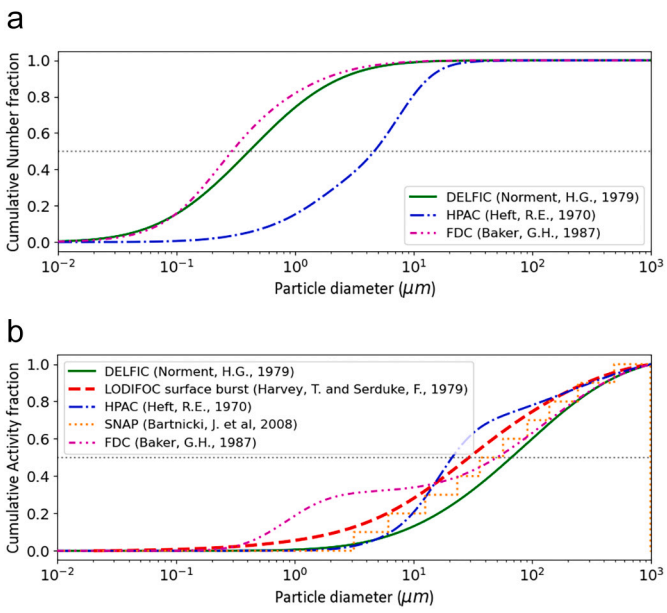


**Fig. 5.** Normalized cumulative size distributions from a near-surface burst for (a) number and (b) activity concentration assumed by each nuclear fallout model shows that similar NSDs (e.g. DELFIC and FDC) will result in different effects because of their distinct ASDs. LODIFOC and SNAP number size distributions are not shown since they define fallout in terms of the radioactivity. FDC and DELFIC utilize NSD with similar small median diameters, but the additional small mode in FDC is apparent with one-third of radioactivity associated with particles smaller than 10 μm.

showed that utilizing different ASDs in a dispersion model varied the model's ability to reproduce the deposition pattern (Rolph et al., 2014). Additionally, these models are computationally inexpensive so they can be used in emergency response situations. However, such predictions may be poor when extrapolated to environments or detonations not representative of the empirical data on which the model inputs are based. By replacing the empirical assumptions with microphysical models that require knowledge of the entrained particle properties, better predictions may be achieved.

### 4.3. *Numerical methods resolving microphysical processes*

An alternative approach to prescribing the NSD or ASD is to utilize mathematical models and numerical methods to simulate fallout size distributions. Numerical methods are utilized to model the effects of microphysical processes (e.g., Eq. (1)) on the particle population size distribution. In these approaches, local conditions can influence the evolution of the particle size distribution. Possible numerical methods include modal, sectional, and Lagrangian techniques. The purpose of this section is not to provide an exhaustive review of different numerical methods to simulate particle size distributions, PSDs, in computer models, but rather to highlight common methods used in related applications that could improve fallout models.

#### 4.3.1. *Modal approach*

The modal approach is often utilized to simulate aerosol, or ambient particle, microphysics in global chemistry (Wilson et al., 2001; Pringle et al., 2010; Mann et al., 2010) and climate (Liu et al., 2012; Easter, 2004; Bellouin et al., 2013) models to predict the effects of particle size distributions on pollution and haze, cloud formation, and other applications.

The modal microphysics scheme separates the particle size distribution into several lognormal modes and assumes that each species or particle type follows a lognormal size distribution. Separating the PSD into separate modes is useful to simulate mixes of different particle types

(e.g. dust, soot, metals) and allows the model to track the evolution of different particle categories (e.g. nucleation, accumulation, coarse modes). A schematic illustrating how the modal approach is used to represent a particle size distribution is shown in Fig. 6a. The full size distribution is separated into three modes, which can be different species or types of particles as shown on the composition axis. Up to three parameters are predicted to describe each mode, which can include the height, mean or median ($\mu$), and width ($\sigma$) of each lognormal mode.

To predict the time-varying parameter of each mode, a selected moment (e.g., total number, surface area, volume of particles) is tracked based on the population balance governing equation by applying the $k^{th}$ moment of particle diameter to Eq. (1) (Whitby and McMurry, 1997; Ackermann et al., 1998). Tracking three moments allows the model to freely evolve the size distribution since a lognormal distribution is explained with three parameters: number concentration, median diameter, standard deviation. If only one (or two) moments are tracked, then two (or one) characteristics of the size distribution must be assumed. It has been shown that a modal approach modeling coagulation and condensational growth that allows the standard deviation to vary provides more accurate predictions than a method prescribing $\sigma$ (Zhang et al., 1999).

Recent work modeling cloud rise post-detonation utilizes the Weather Research and Forecasting (WRF) Model with a 3-moment modal scheme: Modal Aerosol Dynamics model for Europe (MADE) (Arthur et al., 2021). The fallout PSD formed from the airburst was represented by a lognormal distribution with $\mu = 0.07$ $\mu$m and $\sigma = 2$. This approach uses a prescribed particle size distribution then simulates later time microphysics such that clouds, weather, and other influences can modify the size distribution as it evolves. Models enabling feedback to weather- and entrainment-dependent evolution can afford greater fidelity in prediction of fallout ASD and dose rate.

#### 4.3.2. Sectional approach

Sectional microphysics approaches solve the partial differential equations describing particle microphysics in Eq. (1) by discretizing the size distribution into several sections based on particle size defined by their mass or diameter. The sectional technique can be applied to the particle number and mass size distribution to allow flexibility in the particle mass density of each section or "bin". A two-moment sectional approach simulates the number of particles in each bin as well as the mass of each species in each bin so that the total number of variables to describe the particle size distribution is $N_{bin} \times \left(N_{species} + 1\right)$. This is illustrated with the mass moments for a case with $N_{species} = 3$ in Fig. 6b. The number of variables necessary for this technique is significantly higher than the modal technique but offers the advantage of resolving the size distribution evolution more accurately (Zhang et al., 1999, 2020). The sectional approach represents observations better than the modal approach for modeling scenarios such as aerosol coagulation (Zhang et al., 1999), stratospheric aerosol effective radius (Weisenstein et al., 2007), activated aerosol in clouds (Zhang et al., 2002), and free troposphere accumulation to coarse aerosol concentration (Mann et al., 2012). Additionally, several bins may not actually be necessary (many bins have approximate values of zero) for large or small particle sizes of a certain species. This is illustrated by the nearly transparent purple bins in Fig. 6b. Sectional approaches require a tradeoff between computational expense and either truncating the size distribution or reducing the resolution in terms of particle size. Thus, implementing a sectional approach can add to the calculation expense (time to resolve a solution for a fallout model).

The size distribution predicted with the sectional approach does not necessarily follow a lognormal shape, so it can account for the effects of various microphysical processes that may not translate to a lognormal distribution. The sectional approach has been applied to atmospheric particle microphysics in regional and global models. The technique is typically considered too expensive for global climate models, but it has been applied to global chemical transport models (AboEl-Fetouh et al., 2022) and some climate models (Kokkola et al., 2008, 2009; Yu et al., 2015) to achieve a more accurate representation of the particle size distribution shape.

As opposed to the empirical models, sectional approaches can account for environmental conditions in the underlying microphysical process rates determining the evolution of the PSD. This method was applied to modeling particles formed in a chemical explosion (Sreekanth et al., 2020), a scenario that shares many microphysical processes with fallout formation from a nuclear detonation. Although there are significant differences in the explosive energy density and materials. This approach has recently also been utilized to develop a first-principles fallout formation model that assumes constant and uniform fallout particle density using a one-moment sectional approach (Moresco, 2021). Used in this way, relevant microphysics are directly solved rather than prescribed, reducing uncertainties in resultant ASD and dose rate. Chemical composition of vapor species in the fallout cloud and their heterogeneity, vapor pressure, and nucleation rates consequently become primary sources of uncertainty.

#### 4.3.3. Lagrangian approach

Similar to the sectional scheme, a Lagrangian method explicitly simulates the particle size distribution. As the sectional approach is

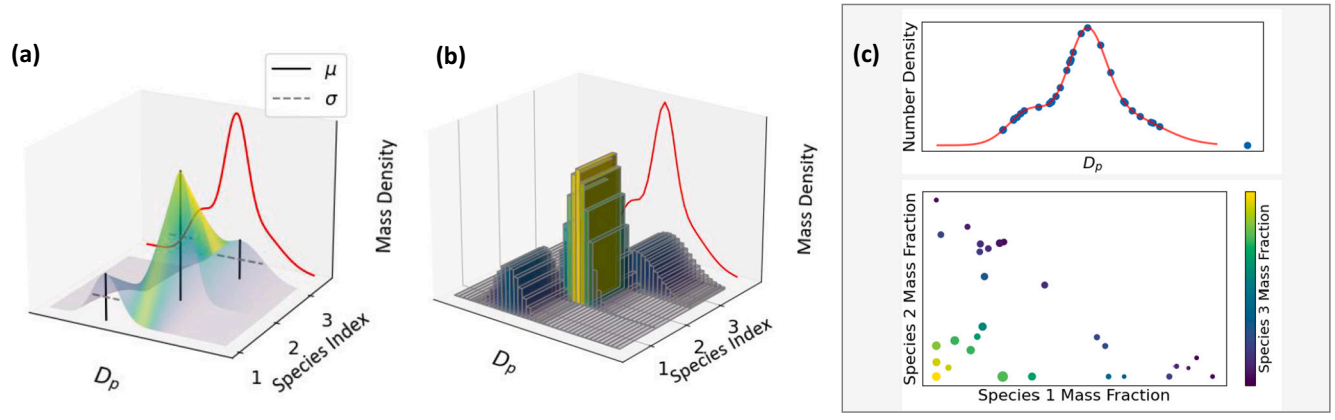


**Fig. 6.** A multi-component particle size distribution modeled by (a) modal, (b) sectional, and (c) Lagrangian techniques. All represent same population in 2- or 3-D. The population is constructed based on the predicted variables of each method including the $\mu$ and $\sigma$ parameters of lognormal distributions for each mode, mass of each bin, and computational particle attributes of size, number density, and mass of each species. In (a) three modes are shown for each species, each of which has 3 prognostic variables. In (b) 40 bins are used to discretize the size distribution of each species. In (c) 40 computational particles are used, which each includes four prognostic attributes.

analogous to an Eulerian grid in which material can pass in and out of pre-defined sections or bins, the Lagrangian method tracks the particle evolution from the reference frame of computation particles representative of several real particles. Instead of modeling the number and/or mass of particles of specified sizes, the Lagrangian technique adjusts the size based on the effect of each microphysical process. For example, modeling condensation with the Lagrangian scheme causes computational particles to grow, whereas in the sectional approach it causes particles to move from smaller to larger bins.

By utilizing a Lagrangian approach, fallout is tracked only where the plume goes and not across the entire domain. The resulting computational savings can be significant since fallout modeling domains can become extensive, especially if aiming to capture the deposition of global fallout. There can be significant additional computational savings over the sectional approach if the size distribution can be represented with fewer computational particles than sectional bins. Implementing this technique may be advantageous over the sectional approach since many fallout post-detonation models are in Lagrangian reference frames. In such cases, these models already contain the infrastructure to model the particle size distribution and just need added attributes and routines to model their microphysical processes.

Several Lagrangian approaches to microphysics have been described in the literature. The Lagrangian Cloud Model was introduced by Andrejczuk et al. (2008), and the super-droplet method (SDM) was introduced by Shima et al. (2009) for cloud microphysics. A Particle Monte Carlo method was introduced by Riemer et al. (2009) for simulating the mixing state of soot in a plume. Fig. 6c shows an example of these approaches, where the multi-component particle population is represented with Lagrangian "super-droplets" or computational particles representing multiple real particles. In the top figure, each circle marker represents the attributes of multiplicity, or the number density of real particles, and the size on the y-axis and x-axis, respectively. The mass fraction attributes are shown in the bottom portion of Fig. 6c with the marker size scaling with each super-droplet's diameter attribute. This results in a more flexible definition of particle size with fewer constraints on the size distribution.

Recent work applied SDM to model nuclear fallout in a homogeneous cloud post-detonation of an airburst (McGuffin et al., 2022). Results detailed the application of SDM to nuclear fallout microphysics for a simple set-up excluding radionuclide activation or decay, ground-interactions, and spatial heterogeneity of the cloud. This work provides a framework for replacing semi-empirical fallout prediction approaches with Lagrangian microphysics.

## 5. Future research directions

The previous section summarized numerical methods that can be used to simulate the evolution of fallout size distributions due to nucleation, coagulation, and condensation. Once formed, fallout can affect processes in the environment such as rain and weather. Feedbacks from weather can correspondingly alter the continuing evolution of fallout. A fully predictive model of post-detonation fallout involves coupling particle microphysics with several other aspects of fallout cloud evolution, including fluid dynamics, radiation, chemistry, thermodynamics, climate, and weather. Incorporating influences from these processes would allow predictive models to account for the various feedback effects. In the following sections we discuss possible next steps in developing a predictive model of post-detonation fallout including the incorporation of microphysical numerical methods, multi-phase hydrodynamics, and atmospheric dynamics and associated chemistry as depicted in Fig. 7.

### 5.1. Including microphysics in fallout models

The first step towards a fully coupled multi-physics model is to utilize microphysical numerical methods for online estimates of the fallout size distribution within currently available nuclear detonation and dispersion models. The approach utilized – modal, sectional, or Lagrangian – depends on the type of nuclear detonation model. The modal approach is ideal for a computationally expensive model, while a sectional or Lagrangian approach may provide better accuracy. A Lagrangian microphysics approach is also optimal for a Lagrangian dispersion model already utilizing computational particles.

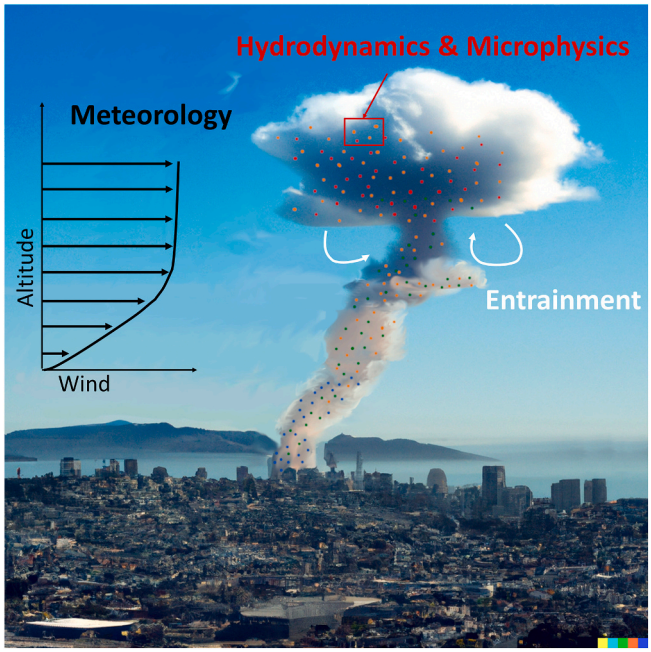


**Fig. 7.** Schematic of future nuclear detonation model including particle microphysics coupled with feedback to processes such as cloud microphysics, momentum, entrainment, and meteorology. Future models will be better able to predict nuclear effects by including more realistic atmospheric dynamics and potentially untested environments. The background image was created with the assistance of DALL·E 2.

Challenges in transitioning from empirical to microphysical predictions of the fallout size distribution include modeling cloud formation and high-temperature chemical and physical properties of debris. Current operational nuclear detonation and dispersion models do not simulate the details of fallout cloud formation and rise. The models generally begin simulation with either (1) an empirically based effective stabilized cloud in which the cloud dimensions and its activity-size distributions are parameterized or (2) a simplified, fast-running time-dependent buoyant cloud rise model (Auxier et al., 2017). Operational models with simplified cloud rise predict the average cloud temperature for semi-empirical particle formation modeling, which is also used to simulate the initial particle rise and spread during cloud rise (Norment, 1979).

Incorporating fallout microphysics into current operational models would require assumptions about cloud temperature and size evolution as the fireball transitions to a fallout cloud and stabilizes. Improved knowledge of relevant thermodynamic equations of state and chemical reactions for materials at conditions relevant to rapid cooling from extreme detonation temperatures is also necessary to inform fallout evolution. Still lacking is an understanding and model-appropriate description of basic thermodynamic and kinetic parameters, such as surface tension and saturation vapor pressure, at temperatures of thousands of Kelvin (at and below the boiling points of relevant species) to predict fallout nucleation and condensation, see Eqs. (2) and (3). Improving the representation of vapor condensation would also improve the fidelity of fractionation predictions and related chemical distributions. Entrainment properties would also need to be accounted for at late times (Lundquist et al., 2023), if applicable, as injection of large soil

particles provides surface area for condensation of any vapors and potentially scavenging of small existing particles via coagulation, see Eqs. (4) and (5).

Adding improved capability for prediction of fallout particle size distribution in post-detonation models would improve the simulated source term for the radioactive debris. Improved model fidelity for diverse environmental conditions would generate more accurate fallout predictions, unconstrained to historic test conditions. Similar developments have occurred in the cloud microphysics field, where modal techniques (also referred to as two-moment schemes) applied to high-resolution numerical weather prediction models start to influence convective motions due to the latent heating and cooling of water droplets (Morrison et al., 2020).

### 5.2. Hydrodynamic multi-phase coupling

Full prediction accounting for the dynamic evolution of fallout composition requires accurate knowledge of the fireball and cloud conditions along with the chemical composition and microphysics of vaporized compounds, both from the device and surrounding materials. This kind of simulation also requires including radiation transport. To achieve this level of fidelity, a predictive model of fallout microphysics can use first-principles instead of assumptions on the cloud cooling and expansion curves. Incorporating the numerical microphysics modeling techniques in a hydrodynamics model with mass and radiation transport would provide improved predictions of the fallout size distribution.

Multiphysics models resolve turbulence and multiple phases as the shock wave interacts and alters the ground. Recent work has developed a numerical approach to simulate multiphase flow regimes across a wide range of Mach numbers, as experienced during a nuclear detonation and cloud formation (Kanarska et al., 2020). In addition to modeling the transition from compressible to incompressible flow, the hydrodynamic model must also include radiation transport to account for particle effects on thermal profiles. Due to the wide range of densities and temperatures in a fireball and cloud, inclusion of radiation transport necessitates data across a large spectral range of opacity of the environment (Morris et al., 2020). Additionally, the gas-phase chemical kinetics of fallout precursors are important to capture due to their effect on nucleation and condensation processes. Recent work presented a kinetics approach to uranium oxide formation (Finko et al., 2017), such an approach could be leveraged with data from laser ablation and plasma flow experiments to constrain time-dependent speciation during fallout evolution (Koroglu et al., 2018, 2022; Burton et al., 2022).

Physics and chemical processes resulting in fallout vary based on the vapor composition, cloud conditions, and the local environment. Coupling chemical reactions with fallout microphysics will enable further exploration of the influence of diverse environments and detonations on cooling and particle activity size distributions. Chemistry effects are observed even in well-understood detonations in the Nevada desert where an airburst cloud is initially red-brown as the detonation produces approximately $10^{32}$ molecules of $NO_x$ per megaton TNT (Glasstone and Dolan, 1977).

The importance of hydrodynamic coupling is depicted by the Grable test simulation described in Section 1 and the debris samples discussed in Section 3. Fig. 1 shows a stabilized cloud prediction in which significant entrainment of large, soil particles up to 4 km above mean sea level is achieved so that overall the fission products were not well-mixed with lofted soil. Including microphysics would enable a model to capture how the fission products combined with soil and accurately predict fallout from this event. Diverse samples in Fig. 4 show evidence of all microphysical processes including condensation, coagulation, and nucleation during ground-interacting events. In particular, Fig. 4(b) and (f) were ground-based and airborne collections. As such, the debris formation and evolution followed different paths, but both show evidence of coagulation. The resultant debris records different microphysical processes and illustrates the value of a fallout microphysics model with hydrodynamic multiphysics able to represent coupling the influence of the environment.

### 5.3. Atmospheric coupling

Representing feedback on the surrounding atmospheric state is another step towards developing a fully coupled fallout model. This can be accomplished by incorporating the post-detonation code with weather or climate models. Some of the potential feedbacks that can be captured include climatic cooling due to smoke, “nuclear winter”, (Coupe et al., 2019; Reisner et al., 2018; Wagman et al., 2020; Redfern et al., 2021) and self-induced rainout or “black rain” (Arthur et al., 2021). “Nuclear winter” is the response of a nuclear war resulting in massive fires, smoke, and decrease in solar radiation at the surface. The ability to predict these effects on the Earth's radiation balance would not necessarily adjust the radioactivity hazard predictions, but it would enable assessments of incidents in a larger context of global climate. Black rain occurs as moist convective flow around the debris-laden fallout cloud forms precipitation altering the weather and hazard predictions. Simulating black rain effects requires a fallout microphysics model that can predict debris sizes in tandem with atmospheric dynamics capturing the convective flow under the local conditions (e.g., water vapor content).

Cloud rise under a realistic atmospheric state with entrainment of ambient air was modeled with the Weather Research and Forecasting (WRF) model in a large-eddy simulation (LES) model (Arthur et al., 2021). This work shows cloud rise modeling results from a LES weather model that agree with observations of U.S. historical airburst nuclear tests. Additionally, the WRF-LES produces self-induced rainout in a semi-idealized simulation representing the detonation over Nagasaki, Japan on August 9, 1945. Predicting the same event in current fallout codes, absent of atmospheric coupling and knowledge of the rainout process, would result in a total exposure rate that would be decreased as the particles continue to stay aloft until settling. This implementation prescribed a fallout size distribution based on prior measurements from historical airburst nuclear tests. Incorporating fallout microphysics in nuclear detonation simulations with atmospheric models improves the accuracy of outputs including deposition rates and allows the prediction of regional and global scale impacts.

## 6. Summary and recommendations

Incorporation of fallout microphysics into predictive models is the next step to achieving accurate models of fallout characteristics under diverse conditions. Particle microphysics describe the formation and evolution of particles by representing entrainment of environmental materials, nucleation, condensation, coagulation, and loss due to wet and dry deposition. Observed debris microstructures and compositions point towards diverse microphysical processes occurring during fallout formation and evolution. Current post-detonation fallout models prescribe the particle or activity size distribution based on measurements primarily in Nevada. These models release a particle size distribution in the post-detonation cloud and simulate their deposition as the cloud disperses. Resulting fallout size and deposition pattern are not necessarily representative of a specific detonation without including entrainment, nucleation, condensation, and coagulation. Approaches described here offer options for more realistic representation of these essential characteristics.

Modeling techniques demonstrated across different scientific fields show how particle microphysics can be leveraged in fallout post-detonation codes. Numerical methods that have been successful with atmospheric aerosol or cloud microphysics include the modal, sectional, and Lagrangian approaches. A promising Lagrangian approach has been utilized for modeling fallout from an airburst in a homogeneous cloud. Such work could be extended to include entrainment of ground materials or to simulate microphysics in a three-dimensional model.

Incorporating fallout microphysics into a three-dimensional dispersion or hydrodynamic model would be a significant step towards a predictive fallout microphysics model that can simulate fallout under diverse environments. The direction of future work should aim to develop a fully coupled model incorporating post-detonation fallout, chemistry, weather, and climate. Computational simulations of such coupled processes would enable the study of various phenomena including long-term climate effects of nuclear detonations.

## CRediT authorship contribution statement

**D.L. McGuffin:** Writing – review & editing, Writing – original draft, Investigation, Formal analysis, Conceptualization. **D.D. Lucas:** Writing – review & editing, Writing – original draft, Supervision, Conceptualization. **E. Balboni:** Writing – review & editing, Resources. **J.S. Nasstrom:** Writing – review & editing, Writing – original draft. **K.A. Lundquist:** Writing – review & editing, Funding acquisition. **K.B. Knight:** Writing – review & editing, Supervision, Funding acquisition, Conceptualization.

## Declaration of competing interest

The authors declare that they have no known competing financial interests or personal relationships that could have appeared to influence the work reported in this paper.

## Data availability

No data was used for the research described in the article.

## Acknowledgments

This work was performed under the auspices of the U.S. Department of Energy by Lawrence Livermore National Laboratory under Contract DE-AC52-07NA27344 with IM release number LLNL-JRNL-864802. This work was partially funded by Laboratory Directed Research and Development Strategic Initiative projects “Influence of the Environment on Post-Detonation Chemistry and Debris Formation” and “Accelerated Atmospheric Simulations for Rapid Response in Nuclear, Climate, and Energy-Security Applications” with tracking codes 20-SI-006 and 24-SI-001, respectively. A portion of this work was sponsored by the National Nuclear Security Administration, Office of Defense Nuclear Nonproliferation R&D.

Fig. 1 is reprinted from Journal of Environmental Radioactivity, 270, K.A. Lundquist, R.S. Arthur, S. Neuscamman, J.P. Morris, C.R. Scullard, A.W. Cook, N.G. Wimer, P. Goldstein, G.D. Spriggs, L.G. Glascoe, J.S. Nasstrom, Examining the effects of soil entrainment during nuclear cloud rise on fallout predictions using a multiscale atmospheric modeling framework, Pages 107299, Copyright (2023), with permission from Elsevier. Fig. 4(a) and (d) are provided by K. B. Knight. Fig. 4(b) and (e) are reprinted from Geochim. Cosmochim. Ac., 201/15, D. G. Weisz, B. Jacobsen, N. E. Marks, K. B. Knight, B. H. Isselhardt, J. E. Matzel, P. K. Weber, S. G. Prussin, I. D. Hutcheon, Deposition of vaporized species onto glassy fallout from a near-surface nuclear test, 410–426, Copyright (2017), with permission from Elsevier. Fig. 4(c) is reprinted from J. Environ. Radioactiv., 237, T. Genda, K. Knight, Z. R. Dai, E. Balboni, B. L. Goldblum, P. Hosemann, Iron-rich microstructure records of high temperature multi-component silicate melt behavior in nuclear fallout, 106700, Copyright (2021), with permission from Elsevier. Fig. 4(f) is reprinted from E. Balboni, Z. Dai, J. Matzel, M. G. Ferrier, K. Knight, Journal of Radioanalytical and Nuclear Chemistry 331, pp 5371–5379, 2022, Springer Nature.

## Appendix A. Freiling-Tompkins activity-size distribution model with fractionation

In the Freilling-Tompkins model (Tompkins, 1968; Norment, 1979), a fireball temperature vs. time curve (from a model or an equation) is used to determine the time, $t_b$, at which the carrier material reaches its boiling point temperature, $T_b$ (that is, at the time the carrier material condenses from vapor to liquid state). The Bateman equations are used to determine the number of atoms of each radionuclide present at $T_b$, given the initial inventory of fission-product radionuclides. Each radionuclide is classified as refractory or volatile based on if their oxide's boiling point temperature is greater or less, respectively, than $T_b$. The total number of refractory atoms, $Nr$, and the number of volatile atoms, $Nv$, in a mass chain at time $t_b$ are used to determine the index $b_i$.

$$F_R = \frac{Nr}{Nr + Nv} \tag{A.1}$$

$$b_i = \sqrt{F_R} \tag{A.2}$$

Using a tabular particle-size distribution with $n$ size classes, the equivalent fissions of mass chain $i$ for a particle diameter $\delta$ size class $k$ is

$$F_i(\delta_k) = \frac{F_T E_i}{1 + E_i D^{b_i - 1}} \left( \delta_k^{b_i - 1} + D^{b_i - 1} \right) f_M(\delta_k) \tag{A.3}$$

$$E_i = 1 \Big/ \sum_{k=1}^{n} \left( f_M(\delta_k) \delta_k^{b_i - 1} \right) \tag{A.4}$$

based on the total number of equivalent fissions $F_T$, cut-off diameter $D$ set to 100 $\mu$m based on fallout observations, and the mass fraction in size class $k$ $f_M(\delta_k)$. (Note: In the original references (Tompkins, 1968; Norment, 1979), the equations for $F_i$ appear to incorrectly and unintentionally include $Y_i$, the fission yield of the $i^{th}$ mass chain, in the right hand side of the $F_i$ equation.) The geometric mean diameter of particles in size class $k$ is $\delta_k$. The fraction of all the equivalent fissions for mass chain i that are on particle size class $k$ is as follows:

$$f_i(\delta_k) = N_k \delta_k^{b_i + 2} \Big/ \sum_{k=1}^{n} N_k \delta_k^{b_i + 2} \tag{A.5}$$

where $N_k$ is the number of particle in size class $k$. Note that $F_i(\delta_k) = F_T f_i(\delta_k)$.

## References


AboEl-Fetouh, Y., O'Neill, N., Kodros, J., Pierce, J., Lu, H., Ranjbar, K., Xian, P., 2022. Seasonal comparisons of GEOS-Chem-TOMAS (GCT) simulations with AERONET-inversion retrievals over sites in the north american and european arctic. Atmos. Environ. 271, 118852. URL: https://www.sciencedirect.com/science/article/pii/S1352231021006749 https://doi.org/10.1016/j.atmosenv.2021.118852.

Ackermann, I.J., Hass, H., Memmesheimer, M., Ebel, A., Binkowski, F.S., Shankar, U., 1998. Modal aerosol dynamics model for Europedevelopment and first applications. Atmos. Environ. 32, 2981–2999. URL: http://linkinghub.elsevier.com/retrieve/pii/S1352231098000065 https://doi.org/10.1016/S1352-2310(98)00006-5.

Andrejczuk, M., Reisner, J.M., Henson, B., Dubey, M.K., Jeffery, C.A., 2008. The potential impacts of pollution on a nondrizzling stratus deck: does aerosol number matter more than type? J. Geophys. Res. Atmos. 113 https://doi.org/10.1029/2007JD009445. URL: https://agupubs.onlinelibrary.wiley.com/doi/abs/10.1029/2007JD009445.

Arthur, R.S., Lundquist, K.A., Mirocha, J.D., Neuscamman, S., Kanarska, Y., Nasstrom, J. S., 2021. Simulating nuclear cloud rise within a realistic atmosphere using the weather research and forecasting model. Atmos. Environ. 254, 118363. URL: https://www.sciencedirect.com/science/article/pii/S1352231021001813 https://doi.org/10.1016/j.atmosenv.2021.118363.

Auxier, J.P., Auxier, J.D., Hall, H.L., 2017. Review of current nuclear fallout codes. J. Environ. Radioact. 171, 246252. URL: https://www.sciencedirect.com/science/article/pii/S0265931X16303952 https://doi.org/10.1016/j.jenvrad.2017.02.010.

Baker, G.H., 1987. Implications of Atmospheric Test Fallout Data for Nuclear Winter (Ph. D. thesis). Air Force Institute of Technology. URL: https://www.osti.gov/biblio/6091856.

Balboni, E., Dai, Z.R., Ferrier, J.M.M.G., Knight, K., 2022. Chemical and structural characterization of particulate fallout isolated from air-filters. J. Radioanal. Nucl. Chem. 5371–5379. URL: 10.1007/s10967-022-08442-7. https://doi.org/10.1007/s10967-022-08442-7.

Bartnicki, J., Saltbones, J., 2008. Modelling atmospheric dispersion of radioactive debris released in case of nuclear explosion using the Norwegian SNAP model. Croatian Meteorological Journal 43, 111–115. URL: https://hrcak.srce.hr/en/64173.

Bellouin, N., Mann, G.W., Woodhouse, M.T., Johnson, C., Carslaw, K.S., Dalvi, M., 2013. Impact of the modal aerosol scheme GLOMAP-mode on aerosol forcing in the Hadley Centre Global Environmental Model. Atmospheric Chemistry and Physics 13, 3027–3044. URL: https://acp.copernicus.org/articles/13/3027/2013/ https://doi.org/10.5194/acp-13-3027-2013.

Bridgman, C., Bigelow, W., 1982. A new fallout prediction model. Health Phys. 43, 205–218. URL: 10.1097/00004032-198208000-00002. https://doi.org/10.1097/00004032-198208000-00002.

Burton, M.A., Auner, A.W., Crowhurst, J.C., Boone, P.S., Finney, L.A., Weisz, D.G., Koroglu, B., Jovanovic, I., Radousky, H.B., Knight, K.B., 2022. The effect of oxygen concentration on the speciation of laser ablated uranium. Sci. Rep. 12, 2045–2322. https://doi.org/10.1038/s41598-022-07834-9.

Coupe, J., Bardeen, C.G., Robock, A., Toon, O.B., 2019. Nuclear winter responses to nuclear war between the United States and Russia in the whole atmosphere community climate model version 4 and the Goddard Institute for Space Studies Modele. J. Geophys. Res. Atmos. 124, 8522–8543. URL: https://agupubs.onlinelibrary.wiley.com/doi/abs/10.1029/2019JD030509 https://doi.org/10.1029/2019JD030509.

Easter, R.C., 2004. MIRAGE: model description and evaluation of aerosols and trace gases. J. Geophys. Res. 109, D20210 https://doi.org/10.1029/2004JD004571.

Emerson, E.W., Hodshire, A.L., DeBolt, H.M., Bilsback, K.R., Pierce, J.R., McMeeking, G. R., Farmer, D.K., 2020. Revisiting particle dry deposition and its role in radiative effect estimates. Proceedings of the National Academy of Sciences 117, 26076–26082. URL: https://www.pnas.org/doi/abs/10.1073/pnas.2014761117 https://doi.org/10.1073/pnas.2014761117.

English, J.M., Toon, O.B., Mills, M.J., 2013. Microphysical simulations of large volcanic eruptions: Pinatubo and Toba. J. Geophys. Res. Atmos. 118, 1880–1895. URL: https://agupubs.onlinelibrary.wiley.com/doi/abs/10.1002/jgrd.50196 https://doi.org/10.1002/jgrd.50196.

Ermak, D.L., Nasstrom, J.S., 2000. A Lagrangian stochastic diffusion method for inhomogeneous turbulence. Atmos. Environ. 34, 1059–1068. URL: https://www.sciencedirect.com/science/article/pii/S1352231099003799 https://doi.org/10.1016/S1352-2310(99)00379-9.

Farley, F.J.M., 1952. The theory of the condensation of supersaturated ionfree vapour. Proc. R. Soc. Lond. A 212, 530–542. https://doi.org/10.1098/rspa.1952.0099.

Ferlic, K.P., 1983. Fallout: Its Characteristics and Management. Technical Report. Armed Forces Raiobology Research Institute, Bethesda, MD, United States. URL: https://apps.dtic.mil/sti/citations/ADA140111.

Finko, M.S., Curreli, D., Weisz, D.G., Crowhurst, J.C., Rose, T.P., Koroglu, B., Radousky, H.B., Armstrong, M.R., 2017. A model of early formation of uranium molecular oxides in laser-ablated plasmas. J. Phys. D Appl. Phys. 50, 485201. URL: https://doi.org/10.1088/1361-6463/aa92f5.

Freiling, E.C., 1961. Radionuclide fractionation in bomb debris. Science 133, 1991–1998. URL: http://www.jstor.org/stable/1707301.

Freiling, E.C., 1963. Fractionation. III. Estimation of degree of fractionation and radionuclide partition for nuclear debris. In: Technical Report. Naval Radiological Defense Laboratory, San Francisco, CA, United States. URL: https://www.osti.gov/biblio/4119916.

Fuchs, N.A., 1964. The Mechanics of Aerosols. Dover Publications, Inc., New York.

Genda, T., Knight, K., Dai, Z.R., Balboni, E., Goldblum, B.L., Hosemann, P., 2021. Iron-rich microstructure records of high temperature multi-component silicate melt behavior in nuclear fallout. J. Environ. Radioact. 237, 106700. URL: https://www.sciencedirect.com/science/article/pii/S0265931X21001727 https://doi.org/10.1016/j.jenvrad.2021.106700.

Gillespie, D.T., 1975. An exact method for numerically simulating the stochastic coalescence process in a cloud. J. Atmos. Sci. 32, 1977–1989. https://doi.org/10.1175/1520-0469(1975)032<1977:AEMFNS> 2.0.CO;2.

Girshick, S.L., 1994. Particle nucleation and growth in thermal plasmas. Plasma Sources Sci. Technol. 3, 388. URL: https://doi.org/10.1088/0963-0252/3/3/023.

Glasstone, S., Dolan, P.J., 1977. The Effects of Nuclear Weapons, Third edition. United States Department of Defense and the Energy Research & Development Administration. URL: https://www.osti.gov/biblio/6852629 https://doi.org/10.2172/6852629.

Goumans, T.P.M., Bromley, S.T., 2012. Efficient nucleation of stardust silicates via heteromolecular homogeneous condensation. Mon. Not. R. Astron. Soc. 420, 3344–3349. URL: https://doi.org/10.1111/j.1365-2966.2011.20255.x.

Harvey, T., Serduke, F., 1979. Fallout Model for System Studies. Technical Report. Lawrence Livermore National Laboratory, Livermore, CA, United States. URL: https://www.osti.gov/servlets/purl/5708584.

Heft, R.E., 1970. The Characterization of Radioactive Particles From Nuclear Weapons Tests. American Chemical Society Publications, pp. 254–281 chapter 14. URL: https://pubs.acs.org/doi/abs/10.1021/ba-1970-0093.ch014 https://doi.org/10.1021/ba-1970-0093.ch014.

Hicks, H.G., 1982. Calculation of the concentration of any radionuclide deposited on the ground by offsite fallout from a nuclear detonation. Health Phys. 42, 585–600. https://doi.org/10.1097/00004032-198205000-00003.

Jacobson, M.Z., 2003. Development of mixed-phase clouds from multiple aerosol size distributions and the effect of the clouds on aerosol removal. Journal of Geophysical Research: Atmospheres 108. https://doi.org/10.1029/2002JD002691. URL: https://agupubs.onlinelibrary.wiley.com/doi/abs/10.1029/2002JD002691. (arXiv:https://agupubs.onlinelibrary.wiley.com/doi/pdf/10.1029/2002JD002691).

Kanarska, Y., Dunn, T., Glascoe, L., Lundquist, K., Noble, C., 2020. Semi-implicit method to solve compressible multiphase fluid flows without acoustic time step restrictions. Comput. Fluids 210, 104651. URL: https://www.sciencedirect.com/science/article/pii/S004579302030222X https://doi.org/10.1016/j.compfluid.2020.104651.

Kautz, E.J., Weerakkody, E.N., Finko, M.S., Curreli, D., Koroglu, B., Rose, T.P., Weisz, D. G., Crowhurst, J.C., Radousky, H.B., DeMagistris, M., Sinha, N., Levin, D.A., Dreizin, E.L., Phillips, M.C., Glumac, N.G., Harilal, S.S., 2021. Optical spectroscopy and modeling of uranium gasphase oxidation: Progress and perspectives. Spectrochim. Acta B At. Spectrosc. 185, 106283. URL: https://www.sciencedirect.com/science/article/pii/S0584854721002408 https://doi.org/10.1016/j.sab.2021.106283.

Kirkby, J., Curtius, J., Almeida, J., Dunne, E., Duplissy, J., Ehrhart, S., Franchin, A., Gagné, S., Ickes, L., Kürten, A., Kupc, A., Metzger, A., Riccobono, F., Rondo, L., Schobesberger, S., Tsagkogeorgas, G., Wimmer, D., Amorim, A., Bianchi, F., Kulmala, M., 2011. Role of sulphuric acid, ammonia and galactic cosmic rays in atmospheric aerosol nucleation. Nature 476, 429–433. URL: https://doi.org/10.1038/nature10343.

Kokkola, H., Korhonen, H., Lehtinen, K.E.J., Makkonen, R., Asmi, A., Järvenoja, S., Anttila, T., Partanen, A., Kulmala, M., Järvinen, H., Laaksonen, A., Kerminen, V., 2008. SALSA – a sectional aerosol module for large scale applications. Atmos. Chem. Phys. 8, 2469–2483. URL: https://acp.copernicus.org/articles/8/2469/2008/ https://doi.org/10.5194/acp-8-2469-2008.

Kokkola, H., Hommel, R., Kazil, J., Niemeier, U., Partanen, A.I., Feichter, J., Timmreck, C., 2009. Aerosol microphysics modules in the framework of the ECHAM5 climate model – intercomparison under stratospheric conditions. Geosci. Model Dev. 2, 97–112. URL: https://gmd.copernicus.org/articles/2/97/2009/ https://doi.org/10.5194/gmd-2-97-2009.

Koroglu, B., Wagnon, S., Dai, Z., Crowhurst, J.C., Armstrong, M.R., Weisz, D., Mehl, M., Zaug, J.M., Radousky, H.B., Rose, T.P., 2018. Gas phase chemical evolution of uranium, aluminum, and iron oxides. Sci. Rep. 8, 2045–2322. URL: https://doi.org/10.1038/s41598-018-28674-6.

Koroglu, B., Finko, M., Saggese, C., Wagnon, S., Foster, S., McGuffin, D., Lucas, D., Rose, T.P., Crowhurst, J.C., Weisz, D.G., Radousky, H.B., Curreli, D., Knight, K.B., 2022. The influence of cooling rate on condensation of iron, aluminum, and uranium oxide nanoparticles. J. Aerosol Sci. 162, 105959. URL: https://www.sciencedirect.com/science/article/pii/S0021850222000088 https://doi.org/10.1016/j.jaerosci.2022.105959.

Korts, R., Norman, J.H., 1967. A calculational model for condensed state diffusion controlled fission product absorption during fallout formation. In: Technical Report. Naval Radiological Defense Laboratory, San Francisco, CA.

Kuran, P., 2006. How to Photograph an Atomic Bomb. VCE, Inc.

Kwapis, E.H., Villa-Aleman, E., Hartig, K.C., 2023. Spectroscopic signatures and oxidation characteristics of nanosecond laser-induced cerium plasmas. Spectrochimica Acta Part B: Atomic Spectroscopy 200, 106610. URL: https://www.sciencedirect.com/science/article/pii/S0584854722002543 https://doi.org/10.1016/j.sab.2022.106610.

Larson, D.J., Nasstrom, J.S., 2002. Shared- and distributed-memory parallelization of a lagrangian atmospheric dispersion model. Atmos. Environ. 36, 1559–1564. URL: https://www.sciencedirect.com/science/article/pii/S1352231001005404 https://doi.org/10.1016/S1352-2310(01)00540-4.

Lewis, L., Knight, K., Matzel, J., Prussin, S., Zimmer, M., Kinman, W., Ryerson, F., Hutcheon, I., 2015. Spatially-resolved analyses of aerodynamic fallout from a uranium-fueled nuclear test. J. Environ. Radioact. 148, 183–195. URL: https://www.sciencedirect.com/science/article/pii/S0265931X15001241 https://doi.org/10.1016/j.jenvrad.2015.04.006.

Liu, X.Y., 2000. Heterogeneous nucleation or homogeneous nucleation? J. Chem. Phys. 112, 9949–9955. URL: https://doi.org/10.1063/1.481644.

Liu, X., Easter, R.C., Ghan, S.J., Zaveri, R., Rasch, P., Shi, X., Lamarque, J.F., Gettelman, A., Morrison, H., Vitt, F., Conley, A., Park, S., Neale, R., Hannay, C., Ekman, A.M.L., Hess, P., Mahowald, N., Collins, W., Iacono, M.J., Bretherton, C.S., Flanner, M.G., Mitchell, D., 2012. Toward a minimal representation of aerosols in climate models: description and evaluation in the community atmosphere model CAM5. Geosci. Model Dev. 5, 709–739. URL: https://gmd.copernicus.org/articles/5/709/2012/ https://doi.org/10.5194/gmd-5-709-2012.

Lundquist, K.A., Arthur, R.S., Neuscamman, S., Morris, J.P., Scullard, C.R., Cook, A.W., Wimer, N.G., Goldstein, P., Spriggs, G.D., Glascoe, L.G., Nasstrom, J.S., 2023. Examining the effects of soil entrainment during nuclear cloud rise on fallout predictions using a multiscale atmospheric modeling framework. J. Environ. Radioact. 270, 107299 https://doi.org/10.1016/j.jenvrad.2023.107299.

Machta, L., List, R.J., Hubert, L.F., 1956. World-wide travel of atomic debris. Science 124, 474–477. URL: https://www.science.org/doi/abs/10.1126/science.124.3220.474 https://doi.org/10.1126/science.124.3220.474.

Mann, G.W., Carslaw, K.S., Spracklen, D.V., Ridley, D.A., Manktelow, P.T., Chipperfield, M.P., Pickering, S.J., Johnson, C.E., 2010. Description and evaluation of GLOMAP-mode: a modal global aerosol microphysics model for the UKCA composition-climate model. Geosci. Model Dev. 3, 519–551. https://doi.org/10.5194/gmd-3-519-2010.

Mann, G.W., Carslaw, K.S., Ridley, D.A., Spracklen, D.V., Pringle, K.J., Merikanto, J., Korhonen, H., Schwarz, J.P., Lee, L.A., Manktelow, P.T., Woodhouse, M.T., Schmidt, A., Breider, T.J., Emmerson, K.M., Reddington, C.L., Chipperfield, M.P., Pickering, S.J., 2012. Intercomparison of modal and sectional aerosol microphysics representations within the same 3-D global chemical transport model. Atmospheric Chemistry and Physics 12, 4449–4476. URL: https://acp.copernicus.org/articles/12/4449/2012/ https://doi.org/10.5194/acp-12-4449-2012.

Martin, C.R., 1983. Fallout Fractionation in Silicate Soils (Ph.D. thesis). Air Force Institute of Technology. URL: https://apps.dtic.mil/sti/citations/ADA159226.

McGuffin, D.L., Lucas, D.D., Morris, J.P., Spriggs, G.D., Knight, K.B., 2022. Super-droplet method to simulate lagrangian microphysics of nuclear fallout in a homogeneous cloud. J. Geophys. Res. Atmos. 127, e2022JD036599 https://doi.org/10.1029/2022JD036599.

Meyer, C., Deglon, D., 2011. Particle collision modeling – a review. Miner. Eng. 24, 719–730. URL: https://www.sciencedirect.com/science/article/pii/S089268751100104X https://doi.org/10.1016/j.mineng.2011.03.015.

Miller, C., 1960. A theory of formation of fallout from land-surface nuclear detonations and decay of the fission products. In: Technical Report. Naval Radiological Defense Laboratory, San Francisco, CA.

Molenkamp, C.R., 1979. Introduction to self-induced rainout. In: Technical Report. Lawrence Livermore National Laboratory, Livermore, CA, United States. https://doi.org/10.2172/6163450. URL:

Moresco, P., 2021. Description of nucleation, growth and coagulation processes in the modeling of debris formation after a nuclear burst. In: Technical Report. Oak Ridge National Laboratory. Oak, Ridge, TN, United States. URL: https://www.osti.gov/biblio/1760119 https://doi.org/10.2172/1760119.

Morris, J., Shestakov, A., Nichols, A., Isaac, B., B., K.K., 2020. Challenges in simulating ground interacting nuclear explosions. Countering Weapons of Mass Destruction 21, 128–144. URL: https://www.nec.belvoir.army.mil/usanca/CWMDJournal/CWMD%20Journal%20Issue%2021.pdf.

Morrison, H., van Lier-Walqui, M., Fridlind, A.M., Grabowski, W.W., Harrington, J.Y., Hoose, C., Korolev, A., Kumjian, M.R., Milbrandt, J.A., Pawlowska, H., Posselt, D.J., Prat, O.P., Reimel, K.J., Shima, S.I., van Diedenhoven, B., Xue, L., 2020. Confronting the challenge of modeling cloud and precipitation microphysics. Journal of Advances in Modeling Earth Systems 12. https://doi.org/10.1029/2019MS001689 e2019MS001689. URL: https://agupubs.onlinelibrary.wiley.com/doi/abs/10.1029/2019MS001689.

Nasstrom, J.S., Sugiyama, G., Baskett, R.L., Larsen, S.C., Bradley, M.M., 2007. The National Atmospheric Release Advisory Center (NARAC) modeling and decision support system for radiological and nuclear emergency preparedness and response. Int. J. Emerg. Manag. 4, 524–550. https://doi.org/10.1504/IJEM.2007.014301.

Nathans, M.W., Thews, R., Holland, W.D., Benson, P.A., 1970. Particle size distribution in clouds from nuclear airbursts. Journal of Geophysical Research (1896-1977) 75, 7559–7572. URL. https://agupubs.onlinelibrary.wiley.com/doi/abs/10.1029/JC075i036p07559. https://doi.org/10.1029/JC075i036p07559.

DELFIC: Department of Defense fallout prediction system. Volume I - fundamentals. In: Norment, H.G. (Ed.), 1979. Technical Report. Atmospheric Science Associates, Bedford, Massachusetts, United States. URL: https://www.osti.gov/biblio/6606853.

O'Day, B.E., 2009. Estimation of Weapon Yield from Inversion of Dose Rate Contours (Master's thesis). Air Force Institute of Technology. URL: https://scholar.afit.edu/etd/2454.

Pringle, K.J., Tost, H., Message, S., Steil, B., Giannadaki, D., Nenes, A., Fountoukis, C., Stier, P., Vignati, E., Lelieveld, J., 2010. Description and evaluation of GMXe: a new aerosol submodel for global simulations (v1). Geosci. Model Dev. 3, 391–412. URL: https://gmd.copernicus.org/articles/3/391/2010/ https://doi.org/10.5194/gmd-3-391-2010.

Redfern, S., Lundquist, J.K., Toon, O.B., Muñoz-Esparza, D., Bardeen, C.G., Kosović, B., 2021. Upper troposphere smoke injection from large areal fires. J. Geophys. Res. Atmos. 126 https://doi.org/10.1029/2020JD034332.e2020JD034332 2020JD034332 e2020JD034332. URL: https://agupubs.onlinelibrary.wiley.com/doi/abs/10.1029/2020JD034332.

Reisner, J., D'Angelo, G., Koo, E., Even, W., Hecht, M., Hunke, E., Comeau, D., Bos, R., Cooley, J., 2018. Climate impact of a regional nuclear weapons exchange: an improved assessment based on detailed source calculations. J. Geophys. Res. Atmos. 123, 2752–2772. URL: https://agupubs.onlinelibrary.wiley.com/doi/abs/10.1002/2017JD027331 https://doi.org/10.1002/2017JD027331.

Riemer, N., West, M., Zaveri, R.A., Easter, R.C., 2009. Simulating the evolution of soot mixing state with a particle-resolved aerosol model. J. Geophys. Res. Atmos. 114 https://doi.org/10.1029/2008JD011073. URL: https://agupubs.onlinelibrary.wiley.com/doi/abs/10.1029/2008JD011073.

Rolph, G., Ngan, F., Draxler, R., 2014. Modeling the fallout from stabilized nuclear clouds using the HYSPLIT atmospheric dispersion model. J. Environ. Radioact. 136, 41–55. URL: https://www.sciencedirect.com/science/article/pii/S0265931X14001453.

Seinfeld, J.H., Pandis, S.N., 2006. Atmospheric Chemistry and Physics From Air Pollution to Climate Change, 2nd ed. John Wiley & Sons.

Shima, S., Kusano, K., Kawano, A., Sugiyama, T., Kawahara, S., 2009. The super-droplet method for the numerical simulation of clouds and precipitation: a particle-based and probabilistic microphysics model coupled with a non-hydrostatic model. Q. J. Roy. Meteorol. Soc. 135, 1307–1320. URL: https://rmets.onlinelibrary.wiley.com/doi/abs/10.1002/qj.441.

Simon, S.L., Bouville, A., Beck, H.L., 2004. The geographic distribution of radionuclide deposition across the continental US from atmospheric nuclear testing. Journal of Environmental Radioactivity 74, 91–105. URL: https://www.sciencedirect.com/science/article/pii/S0265931X04000281.

Skaar, E.T., 2005. A Comparison of the Heft Subsurface and DELFIC Particle Size Distributions and Effects in HPAC (Master's thesis). Air Force Institute of Technology. URL: https://scholar.afit.edu/etd/3744.

Spriggs, G.D., Neuscamman, S., Nasstrom, J.S., Knight, K.B., 2020. Fallout cloud regimes. In: Countering Weapons of Mass Destruction, 21, pp. 103–113. URL: https://www.nec.belvoir.army.mil/usanca/CWMDJournal/CWMD%20Journal%20Issue%2021.pdf.

Sreekanth, B., Anand, S., Ikkurthi, V.R., Chaudhury, P., Sapra, B.K., Mayya, Y.S., Chaturvedi, S., 2020. Evolution of particle metrics in a buoyant aerosol cloud from explosive releases. Aerosol Science and Technology 54, 656–667. URL: https://doi.org/10.1080/02786826.2020.1723788.

Sugiyama, G., Nasstrom, J., Pobanz, B., Foster, K., Simpson, M., Vogt, P., Aluzzi, F., Homann, S., 2012. Atmospheric dispersion modeling: challenges of the Fukushima Daiichi response. Health Phys. 102, 493–508. https://doi.org/10.1097/HP.0b013e31824c7bc9.

Taccogna, F., 2015. Nucleation and growth of nanoparticles in a plasma by laser ablation in liquid. Journal of Plasma Physics 81, 495810509. https://doi.org/10.1017/S0022377815000793.

Tompkins, R., 1968. Department of Defense land fallout prediction system. Volume 5. Particle activity. In: Technical Report. U.S. Army, Nuclear Defense Laboratory, Edgewood Arsenal, MD, United States. URL: https://apps.dtic.mil/sti/citations/AD0832239.

U.S. Department of Energy, 2015. United States Nuclear Tests July 1945 through September 1992. In: Technical Report. National Nuclear Security Administration Nevada Field Office, Las Vegas, NV, United States. URL: https://www.nnss.gov/docs/docs_librarypublications/doe_nv-209_rev16.pdf.

Vishnyakov, V.I., Kiro, S.A., Ennan, A.A., 2011. Heterogeneous ion-induced nucleation in thermal dusty plasmas. J. Phys. D Appl. Phys. 44, 215201. URL: https://doi.org/10.1088/0022-3727/44/21/215201.

Wagman, B.M., Lundquist, K.A., Tang, Q., Glascoe, L.G., Bader, D.C., 2020. Examining the climate effects of a regional nuclear weapons exchange using a multiscale atmospheric modeling approach. J. Geophys. Res. Atmos. 125 https://doi.org/10.1029/2020JD033056 e2020JD033056. URL: https://agupubs.onlinelibrary.wiley.com/doi/abs/10.1029/2020JD033056.

Weisenstein, D.K., Penner, J.E., Herzog, M., Liu, X., 2007. Global 2-D intercomparison of sectional and modal aerosol modules. Atmospheric Chemistry and Physics 7, 2339–2355. URL: https://acp.copernicus.org/articles/7/2339/2007/. https://doi.org/10.5194/acp-7-2339-2007.

Weisz, D.G., Jacobsen, B., Marks, N.E., Knight, K.B., Isselhardt, B.H., Matzel, J.E., Weber, P.K., Prussin, S.G., Hutcheon, I.D., 2017. Deposition of vaporized species onto glassy fallout from a nearsurface nuclear test. Geochim. Cosmochim. Acta 201, 410–426. URL: https://www.sciencedirect.com/science/article/pii/S0016703716306147.

Whitby, E.R., McMurry, P.H., 1997. Modal aerosol dynamics modeling. Aerosol Sci. Tech. 27, 673–688. URL: https://doi.org/10.1080/02786829708965504.

Wilson, J., Cuvelier, C., Raes, F., 2001. A modeling study of global mixed aerosol fields. J. Geophys. Res. Atmos. 106, 34081–34108. https://doi.org/10.1029/2000JD000198.

Wu, T., Chen, S., Chen, P., Li, S., 2023. Clustering and collision of brownian particles in homogeneous and isotropic turbulence. J. Aerosol Sci. 169, 106134. URL: https://www.sciencedirect.com/science/article/pii/S0021850222001707.

Yu, P., Toon, O.B., Bardeen, C.G., Mills, M.J., Fan, T., English, J.M., Neely, R.R., 2015. Evaluations of tropospheric aerosol properties simulated by the community earth system model with a sectional aerosol microphysics scheme. Journal of Advances in Modeling Earth Systems 7, 865–914. https://doi.org/10.1002/2014MS000421.

Yu, F., Nadykto, A.B., Herb, J., Luo, G., Nazarenko, K.M., Uvarova, L.A., 2018. $H_2SO_4$ – $H_2O$ – $NH_3$ ternary ion-mediated nucleation (TIMN): kinetic-based model and comparison with CLOUD measurements. Atmospheric Chemistry and Physics 18, 17451–17474. URL: https://acp.copernicus.org/articles/18/17451/2018/. https://doi.org/10.5194/acp-18-17451-2018.

Zhang, Y., Seigneur, C., Seinfeld, J.H., Jacobson, M.Z., Binkowski, F.S., 1999. Simulation of aerosol dynamics: a comparative review of algorithms used in air quality models. Aerosol Sci. Tech. 31, 487–514. URL: https://doi.org/10.1080/027868299304039.

Zhang, Y., Easter, R.C., Ghan, S.J., Abdul-Razzak, H., 2002. Impact of aerosol size representation on modeling aerosol-cloud interactions. J. Geophys. Res. Atmos. 107. AAC 4–1–AAC 4–17. URL: https://agupubs.onlinelibrary.wiley.com/doi/abs/10.1029/2001JD001549 https://doi.org/10.1029/2001JD001549.

Zhang, H., Sharma, G., Dhawan, S., Dhanraj, D., Li, Z., Biswas, P., 2020. Comparison of discrete, discrete-sectional, modal and moment models for aerosol dynamics simulations. Aerosol Science and Technology 54, 739–760. URL: https://doi.org/10.1080/02786826.2020.1723787.